The pyrrolopyrimidine colchicine-binding site agent PP-13 reduces the metastatic dissemination of invasive cancer cells in vitro and in vivo

Pauline Gilson, Morgane Couvet, Laetitia Vanwonterghem, Maxime Henry, Julien Vollaire, Vladimir Baulin, Marco Werner, Anna Orlowska, Véronique Josserand, Florence Mahuteau-Betzer, et al.

Elsevier Editorial System(tm) for Biochemical Pharmacology

Manuscript Draft

Manuscript Number: BCP-D-18-01133R1

Title: The pyrrolopyrimidine colchicine-binding site agent PP-13 reduces the metastatic dissemination of invasive cancer cells in vitro and in vivo

Article Type: Full Length Articles

Section/Category: Antibiotics and Chemotherapeutics

Keywords: spheroids; invasion; metastasis; drug-refractory tumors; pyrrolopyrimidine

Corresponding Author: Dr. Amandine Hurbin, Ph.D.

Corresponding Author's Institution: INSERM U1209

First Author: Pauline Gilson, PhD, PharmD

Order of Authors: Pauline Gilson, PhD, PharmD; Morgane Couvet; Laetitia Vanwonterghem; Maxime Henry; Julien Vollaire; Vladimir Baulin; Marco Werner; Anna Orlowska; Véronique Josserand; Florence Mahuteau-Betzer; Laurence Lafanechère; Jean-Luc Coll; Benoit Busser; Amandine Hurbin, Ph.D.

Abstract: Standard chemotherapies that interfere with microtubule dynamics are a chemotherapeutic option used for the patients with advanced malignancies that invariably relapse after targeted therapies. However, major efforts are needed to reduce their toxicity, optimize their efficacy, and reduce cancer chemoresistance to these agents. We previously identified a pyrrolo[2,3d]pyrimidine-based microtubule-depolymerizing agent (PP-13) that binds to the colchicine site of β-tubulin and exhibits anticancer properties in solid human cancer cells, including chemoresistant subtypes. Here, we investigated the therapeutic potential of PP-13 in vitro and in vivo. PP-13 induced a mitotic blockade and apoptosis in several cancer cells cultured in two-dimensions or three-dimensions spheroids, in conjunction with reduced cell proliferation. Capillary-like tube formation assays using HUVECs showed that PP-13 displayed antiangiogenic properties. It also inhibited cancer cell motility and invasion, in in vitro wound-healing and transwell migration assays. Low concentration PP-13 (130 nmol.L-1) treatment significantly reduced the metastatic invasiveness of human cancer cells engrafts on chicken chorioallantoic membrane. In nude mice, 0.5 or 1 mg.kg-1 PP-13 intraperitoneally administered three-times a week reduced the sizes of paclitaxel-refractory orthotopic breast tumors, delayed the progression of metastasis, and decreased the global metastatic load compared to 0.5 mg.kg-1 paclitaxel or vehicle alone. PP-13 did not show any apparent early adverse effect in vivo. These data suggest that PP-13 is a promising alternative to standard chemotherapy in antimitotic drug-refractory tumors, especially through its impact on metastasis.

The pyrrolopyrimidine colchicine-binding site agent PP-13 reduces the metastatic dissemination of invasive cancer cells in vitro and in vivo

Pauline Gilson[1,2,#], Morgane Couvet[1], Laetitia Vanwonterghem[1], Maxime Henry[1], Julien Vollaire[1], Vladimir Baulin[3], Marco Werner[3], Anna Orlowska[3], Véronique Josserand[1], Florence Mahuteau-Betzer[4], Laurence Lafanechère[5], Jean-Luc Coll[1], Benoit Busser[1,2,*], Amandine Hurbin[1,*]

[1] Cancer Target and Experimental Therapeutics, Institute for Advanced Biosciences, INSERM U1209, CNRS UMR5309, Grenoble Alpes University, Grenoble, France.

[2] Biochemistry Department, Grenoble University Hospital, Grenoble, France.

[3] Departament d'Enginyeria Quımica, Universitat Rovira i Virgili, Tarragona, Spain.

[4] Institut Curie, PSL Research University, CNRS, INSERM UMR9187/U1196, Orsay, France.

[5] Regulation and Pharmacology of the Cytoskeleton, Institute for Advanced Biosciences, INSERM U1209, CNRS UMR5309, Grenoble Alpes University, Grenoble, France.

[#] Present address: Université de Lorraine, Faculté de Pharmacie; CNRS UMR7039 CRAN, Nancy, France; and Institut de Cancérologie de Lorraine, Service de Biopathologie, Vandoeuvre-lès-Nancy, France.

[*] Co-last authors.

Corresponding authors:

Amandine Hurbin, Institute for Advanced Biosciences, INSERM U1209, CNRS UMR5309, Grenoble Alpes University, Grenoble, France. Tel: +33 4 76 54 95 53. Fax: +33 4 76 54 94 13. amandine.hurbin@inserm.fr.

Benoit Busser, Institute for Advanced Biosciences, INSERM U1209, CNRS UMR5309, Grenoble Alpes University, Grenoble, France. Tel: +33 4 76 54 94 20. Fax: +33 4 76 54 94 13. bbusser@chu-grenoble.fr.

Conflict of interest: The authors have no conflict of interest to declare.

Abstract

Standard chemotherapies that interfere with microtubule dynamics are a chemotherapeutic option used for the patients with advanced malignancies that invariably relapse after targeted therapies. However, major efforts are needed to reduce their toxicity, optimize their efficacy, and reduce cancer chemoresistance to these agents. We previously identified a pyrrolo[2,3d]pyrimidine-based microtubule-depolymerizing agent (PP-13) that binds to the colchicine site of β-tubulin and exhibits anticancer properties in solid human cancer cells, including chemoresistant subtypes. Here, we investigated the therapeutic potential of PP-13 in vitro and in vivo. PP-13 induced a mitotic blockade and apoptosis in several cancer cells cultured in two-dimensions or three-dimensions spheroids, in conjunction with reduced cell proliferation. Capillary-like tube formation assays using HUVECs showed that PP-13 displayed antiangiogenic properties. It also inhibited cancer cell motility and invasion, in in vitro wound-healing and transwell migration assays. Low concentration PP-13 (130 $nmol.L^{-1}$) treatment significantly reduced the metastatic invasiveness of human cancer cells engrafts on chicken chorioallantoic membrane. In nude mice, 0.5 or 1 $mg.kg^{-1}$ PP-13 intraperitoneally administered three-times a week reduced the sizes of paclitaxel-refractory orthotopic breast tumors, delayed the progression of metastasis, and decreased the global metastatic load compared to 0.5 $mg.kg^{-1}$ paclitaxel or vehicle alone. PP-13 did not show any apparent early adverse effect in vivo. These data suggest that PP-13 is a promising alternative to standard chemotherapy in antimitotic drug-refractory tumors, especially through its impact on metastasis.

Keywords: spheroids, invasion, metastasis, paclitaxel, drug-refractory tumors, pyrrolopyrimidine

1. Introduction

Despite recent innovations in targeted anticancer strategies over the last decade, non-selective chemotherapies are still widely used for the clinical management of various patients with advanced malignancies [1]. Microtubules represent one of the most common targets for chemotherapies, as they are crucial for the maintenance of cell shape, intracellular transport, cell motility, and chromosome migration during cell division [2]. Taxanes and vinca-alkaloids are the two main classes of microtubule-targeting agents and are classically known to induce microtubule stabilization and depolymerization, respectively [3]. Therapeutic doses of all compounds from these two families lead to the alteration of the dynamic state of the microtubules, which ultimately induces multipolar divisions and causes cell death [4, 5]. Beyond their cytotoxic activity, most microtubule-binding agents display antimetastatic, antiangiogenic or vascular-disrupting properties, supporting their use as therapeutic agents for cancer treatment [6-8]. However, the troublesome side effects of microtubule inhibitors, particularly myelosuppression and peripheral neurotoxicity, and the emergence of chemoresistance, predominantly from the overexpression of efflux transporters, drastically limits their therapeutic outcomes [3], hence underscoring the need for alternative agents.

We recently identified a novel pyrrolopyrimidine-based microtubule-depolymerizing agent (PP-13) that was effective in vitro on a wide range of human cancer cells [9]. PP-13 has no kinase activity, directly binds to the colchicine binding site of β-tubulin, interferes with microtubule organization and induces spindle multipolarity, transient mitotic cell cycle arrest and apoptosis [9]. Interestingly, in marked contrast to conventional microtubule-damaging drugs, PP-13 escapes resistance mechanisms linked to the presence of efflux pumps, which underlies its *potential* anticancer activity for multidrug-resistant cancer cells [9].

Based on the efficacy of PP-13 against human cancer cell proliferation and multidrug-resistant cancer cells, the aim of the present study was to investigate the therapeutic potential of PP-13 against highly invasive and aggressive cancer cell lines in vitro and in vivo. The effects of PP-13 were analyzed in HeLa cervical cancer cells, A549 NSCLC cells and 4T1 murine mammary cancer cells that were cultured in two-dimensions monolayers or in three-dimensions-spheroids. The impact of PP-13 on cell migration, metastasis and angiogenesis was evaluated. Since no colchicine binding-site agent is currently used in clinic for cancer treatment, we assessed the clinical potential of PP-13 activity in comparison with paclitaxel, a standard anti-mitotic chemotherapy that is routinely used for the treatment of a wide range of solid cancers, and is considered a reference treatment for in vitro and in vivo studies of new microtubule-targeting agents.

2. Material and Methods

2.1. Materials

Paclitaxel was obtained from Sigma-Aldrich (Saint-Quentin-Fallavier, France). PP-13 was obtained from Institut Curie (CNRS Chemical library, 2004 version), as described in [9]. All drugs were dissolved in sterile anhydrous dimethyl sulfoxide (DMSO, Carl Roth, Karlsruhe, Germany) at a 10 $mmol.L^{-1}$ stock solution. Phospho-histone H3 (H3P), and active caspase-3 antibodies were purchased from Cell Signaling Technology (Ozyme, Saint-Quentin-Les-Yvelines, France), and conjugated Alexa Fluor 633 goat anti-rabbit antibodies were from Thermo Fisher Scientific (Saint-Aubin, France).

2.2. Cell lines and culture

The human HeLa and A549 cell lines and the murine 4T1 cells were obtained from the American Type Culture Collection (ATCC, Manassas, VA, USA). HeLa cells expressing mEGFP-α-tubulin and mRFP-H2B (HeLa-EGFP/RFP) were a generous gift from Dr. D. Gerlich [10]. The 4T1 cells were stably transfected with a plasmid expressing the fusion histone H2B-RFP (provided by Dr. C. Albigès-Rizo, Institute for Advanced Biosciences, Grenoble, France) (4T1-RFP) or with the pGL4.50[*luc2*/CMV/Hygro] vector encoding the firefly luciferase reporter gene *luc2* (Promega, Charbonnière, France) (4T1-rvLuc2) using JetPEI (Polyplus Transfection, Illkirch, France) according to the manufacturer's protocol. Transfected cells were selected with G418 antibiotic (Invivogen Europe, Toulouse, France, ant-gn-5) and amplified. All cells were routinely tested for the presence of mycoplasma (MYCOALERT® Mycoplasma Detection Kit, Lonza, Amboise, France) and used within three months after thawing. A549, HeLa, and HeLa-EGFP/RFP cell lines were authenticated by DNA STR profiling (ATCC Cell line Authentication Service, LGC Standard SARL, Manassas, VA, USA). Human umbilical vein endothelial cells (HUVECs, passage two to five; Lonza) were cultured in complete medium of the EGM-2 BulletKit (Lonza, Amboise, France).

2.2.1. Two-dimensions (2D) cell culture

Cells were maintained in culture at 37°C in the appropriate medium with 10% FBS in a 5% CO_2 humidified atmosphere, and the cell morphology was routinely checked.

2.2.2. Three-dimensions (3D) cell culture

Spheroids were generated by plating A549 (4000 cells/well), HeLa-EGFP/RFP (1000 cells/well), or 4T1-RFP (2000 cells/well) cells into 96-well round bottom ultra-low

attachment (ULA) spheroid microplates (Corning, Tewksbury, MA, USA). The spheroid culture was performed in medium with 10% FBS in a humidified atmosphere with 5% CO_2. Spheroid formation and growth were assessed by microscopic examination using an inverted microscope and by imaging the spheroids at each time point.

2.3. In vitro cytotoxicity assays

Cell proliferation assays were conducted in 96-well culture plates. 2D-cultured cells and spheroids were cultured for 24 h and 72 h, respectively, prior to treatment with PP-13 or paclitaxel in medium containing 10% FBS for 72 h. The cell viability was quantified using CELLTITER 96® AQueous One Solution cell proliferation assay (Promega, Charbonnière, France) in 2D cell models or by using the CELLTITER-GLO® 3D Cell Viability Assay (Promega, Charbonnière, France) in spheroids. The drug concentrations required to inhibit cell growth by 50% (IC_{50}) were interpolated from the dose-response curves.

2.4. Immunofluorescence analyses of spheroids

After PP-13 treatment, the spheroids were washed, fixed overnight at 4°C in 4% paraformaldehyde, and then washed, frozen and cut into 7-µm sections before mounting onto SuperFrost UltraPlus slides (Thermo Fisher Scientific, Saint-Aubin, France). Cryosections were rehydrated in PBS-glycine, permeabilized for 1 h in PBS with 2% Triton X-100, washed in PBS-glycine, blocked in 10% goat serum and incubated overnight at 4°C with primary antibodies. The sections were then washed in 0.2% Tween-20/PBS and incubated for 1 h with conjugated secondary antibodies. Hoechst was used to counterstain the cell nuclei.

Fluorescence microscopy was carried out using a confocal microscope (LSM 710; Carl Zeiss,

Jena, Germany). An objective Plan Apochromat 20×/0.8 NA in air and an objective Plan Apochromat 63×/1.4 NA in oil were used. The H3P and active caspase-3 expression levels in spheroids were counted based on color thresholding image adjustment using ImageJ software (NIH, Bethesda, MD, USA) and the images were blinded. The percentage of H3P was calculated as the number of H3P-positive cells in control and PP-13-treated spheroids ($n \geq 7$ as indicated in the figure legends, with three different sections analyzed per spheroid). The percentage of cleaved caspase-3 was calculated as the number of cleaved caspase-3-positive cells in control and treated spheroids ($n \geq 7$ as indicated in the figure legends, with two or three different sections analyzed per spheroid).

2.5. Immunoblotting

Western blot analyses were performed as previously described [11] after protein extraction of ten pooled spheroids per condition and sonication. H3P and actin intensities were quantified using the Image J software and the relative densitometric area for H3P were determined according to actin signal in each condition.

2.6. Wound-healing assay

A549, 4T1-rvLuc2 and HeLa cells were seeded into 96-well plates (15000 cells/well) and allowed to grow for 24 h until confluence. Scratching the surface with a wound maker physically wounded the cell monolayers, and increasing concentrations of PP-13 or DMSO were added into the medium. Images of the cells invading the scratch wound were monitored for 12 h using the IncuCyte S3 Live-Cell analysis system (Essen Bioscience, Hertfordshire, UK). The relative wound density was analyzed using the IncuCyte S3 software.

2.7. Transwell migration and invasion assays

A549, 4T1-rvLuc2 and HeLa cells were plated (75000 cells) on top of a transwell chamber with Matrigel (Corning, Tewksbury, MA, USA) under starvation conditions, and complete medium was added into the well. After 24 h of incubation with PP-13 or DMSO, cells that reached the bottom of the transwell were stained with methylene blue and observed by microscopy (AxioImager M2, Carl Zeiss, Jena, Germany). Ten images were obtained per condition and were blinded for quantification. Cell invasion was quantified using a fully connected, three-layer back-propagation neuronal network, as previously described [12]. Briefly, the input layer of the network was prepared to receive 12 9 12 pixel images, with three-color channels totaling up to 12 9 12 9 3 input neurons. A total of twenty-four neurons in the hidden layer were utilized. The output layer consists of two neurons corresponding to the two classes E (empty space between structures) and S (structure) with respect to which each pixel and its neighborhood were classified. A training set of ~10-20 images of each kind were created for training. An extended training set of ~ five hundred pictures per species was generated by rotating each picture by twenty-four equidistant angles, as well as rescaling to 90, 100, and 110% of the original size. Training was performed by (on average) two thousand forward passes per extended training set picture, with full error back propagations. Feed-forward and error-backward propagations employ well-known sigmoidal characteristics based on the logistic function. The target signals for the two output neurons were [1, 0] corresponding to E, and [0, 1] corresponding to S, respectively.

2.8. In vitro capillary-like tube formation assay

A 15-well Ibidi angiogenesis microslide (Ibidi, ~~81506~~ Clinisciences, Nanterren France) was coated with 10 µL of Matrigel matrix (Corning) and incubated for 30 minutes at 37°C for gel polymerization. Twenty thousand HUVECs were seeded on top of the polymerized gel matrix in complete medium with increasing concentrations of PP-13 or 0.1% DMSO. The microslide was then placed in a 37°C heated stage in a 5% CO_2 humidified atmosphere. Images were acquired after 6 h of incubation by a phase-contrast microscope with an Achromat 5×/0.12 NA objective, blinded and analyzed using the automated WimTube image analysis tool (Wimasis GmbH, Munich, Germany).

2.9. In vivo studies using chick embryo tumor model

A chick embryo tumor growth and metastasis assay (InOvotion, Grenoble, France) was performed as previously described [9]. According to French legislation, no ethical approval is needed for scientific experimentations using oviparous embryos (decree number 2013–118, February 1, 2013; art. R-214–88). Briefly, fertilized white leghorn eggs (SFPA, Hendrix Genetics group, Saint Brieuc, France) were incubated at 38°C with 60% relative humidity for nine days. The chorioallantoic membrane (CAM) was then dropped, and a 1-cm^2 window was cut into the eggshell above the CAM (at day nine). A total of three million A549 cells were added directly onto the CAM of each egg. The eggs were randomly allocated into three groups. Group size was determined based on the expertise of InOvotion showing that $n \geq 15$ was the minimum number of eggs to show significant effects. At day ten, when tumors began to be detectable, the eggs were treated every other day for ten days by adding 100 µL of either 50 µmol.L^{-1} paclitaxel ($n = 17$), 0.13 µmol.L^{-1} PP-13 ($n = 18$), or 0.5% DMSO in PBS (vehicle, $n = 18$) dropwise onto the tumor. The concentration of paclitaxel was chosen as a positive control to induce significant tumor growth inhibition without toxicity for embryos.

The concentration of PP-13 has been arbitrarily chosen according to *in vitro* experiments (IC_{50}) and following the expertise of InOvotion. The upper portion of the CAM was then removed, and the tumors were carefully cut away and weighed. In parallel, a 1-cm^2 portion of the lower CAM was collected, genomic DNA was extracted, and qPCR analysis was performed by using primers specific for genomic human Alu/repetitive sequences [9] to evaluate the number of A549 cells. Finally, scoring the number of dead embryos and looking for morphological or functional abnormalities in the surviving embryos was carried out to evaluate the toxicity of the treatment.

2.10. In vivo studies using mice tumor model

All animal studies were performed in accordance with the European Economic Community guidelines and the "Principles of Laboratory Animal Care" (NIH publication N 86-23 revised 1985) and were approved by the institutional guidelines and the European Community (EU Directive 2010/63/EU) for the use of experimental animals (authorization for the experiment: APAFIS#8854-2017031314338357 v1).

Six-week-old female NMRI nude mice (Janvier Labs, Le Genest-Saint Isle, France) were anesthetized using 4% isoflurane/air for anesthesia induction and 1.5% thereafter, and luciferase-modified mouse 4T1 cancer cells (4T1-rvLuc2 cells, 20000 cells per 50 µL) were injected into the mammary fat pad. The mice were immediately randomly divided into four groups of eight mice, receiving vehicle (0.9% NaCl, 1% DMSO, 30% PEG, 1% Tween-80, referred to as control), 0.5 $mg.kg^{-1}$ paclitaxel, 0.5 $mg.kg^{-1}$ PP-13, or 1 $mg.kg^{-1}$ PP-13. Group size was determined based on our expertise showing that $n \geq 8$ per group was the minimum number of mice to show significant effects on metastases. Based on the results obtained on

chick embryo tumor model showing the effect of PP-13 at very low dose, two low concentrations of PP-13 were chosen (0.5 and 1 $mg.kg^{-1}$). Similar low concentration (0.5 $mg.kg^{-1}$) was chosen for paclitaxel to compared this standard chemotherapy with PP-13, and based on preliminary experiments showing sub-therapeutic effect of 0.5 mg/kg^{-1} paclitaxel on tumor and metastases growth (data not shown). Intraperitoneal administration of 200 µL of treatment was performed three times per week for five weeks. The mice were examined daily for behavior and morbi-mortality and were weighed three times per week. The primary tumor growth was monitored three times per week using a caliper, and the tumor volume was calculated as follows [13]: tumor volume = length x width x 0.4. The thoracic metastasis growth was followed once per week by *in vivo* bioluminescence imaging (IVIS KINETIC, Perkin Elmer, Waltham, MA, USA) 5 min after the intraperitoneal injection of 150 $mg.kg^{-1}$ of luciferin (Promega, E1605), as previously described [14]. Twenty-two days after 4T1-rvLuc2 cell implantation, 0.1 $mg.kg^{-1}$ buprenorphine was injected subcutaneously for analgesia and the primary breast tumors were excised under general anesthesia. The mice were carefully observed during the day following the surgery. After five weeks, the mice were sacrificed and blood samples were collected by cardiac puncture using a heparinized syringe. The lungs, axillary and brachial lymph nodes, kidney and liver were harvested for further imaging and/or analyses.

2.11. Ex vivo studies of mice tissue samples

Blood samples were evaluated for hematological parameters with a medical automated hematology analyzer (Micros-60, Horiba ABX, Montpellier, France), and biochemical analyses were performed by the Charles Rivers Laboratory (Massachusetts, USA). Bone marrow was obtained after having carefully sectioned mice femurs at each joint and flushing

the bone cavity with PBS. Cells from the plasma and bone marrow samples were washed in PBS, cytospun (Cytospin 4, Fisher Scientific, Illkirch, France) and stained with May-Grunwald-Giemsa solution (MGG) with the automated XE-5000 Instrument (Sysmex, Roissy, France). Global cell abundance evaluation and megakaryocyte and leukocyte counting were then performed for both samples by an experienced hematologist.

Tumor tissues were frozen in OCT-embedding medium (VWR international, Fontenay-sous-Bois, France) and cut into 7 µm thick sections using a cryomicrotome for immunohistochemical analyses. Immunohistochemical examinations were performed after fixation with 4% paraformaldehyde and staining with anti-CD31 antibody (Pharmingen, BD Biosciences, Le Pont de Claix, France), using an AxioImager M2 microscope (Carl Zeiss, Jena, Germany). Segmentation of tissues was performed using a fully connected, three-layer back-propagation neuronal network, as previously described [12].

2.12. Statistical analyses

All analyses were performed using the GraphPad Prism software (GraphPad Software Inc., San Diego, California, USA). Statistical comparisons between two groups or more were conducted with Mann-Whitney test, Kruskal-Wallis test, or Friedman test with Dunn's multiple comparisons post hoc test. Statistical comparisons between mice groups among time were determined by two-way ANOVA with Bonferroni's post hoc test. Statistical significance was defined for p values ≤ 0.05.

3. Results

3.1. PP-13 treatment decreases cancer cell proliferation in vitro

To investigate the therapeutic effect of PP-13, we chose three cell lines displaying high levels of proliferation, migration and invasiveness: the human HeLa cervical cell line and its derivative subclone expressing mEGFP-α-tubulin and mRFP-H2B (HeLa-EGFP/RFP), the human A549 lung cancer cell line, and the mouse 4T1 mammary cancer cells expressing mRFP-H2B (4T1-RFP) or luciferase (4T1-rvLuc2). We first analyzed the toxicity of PP-13 in these cell lines cultured in monolayers or in 3D-spheroids. PP-13 had a significant effect on the proliferation of these cell lines, strongly reducing their viability (Fig. 1A). The IC_{50} values of PP-13 (50% growth inhibition) were relatively similar for the three cell lines cultured in monolayers (Table 1) [9]. These IC_{50} values did not vary significantly when the cells were grown in spheroids, except for A549 (Table 1 and Fig. 1A and 1B). Indeed, the A549 spheroids appeared to strongly resist PP-13 treatment compared to A549 cells in the monolayer cell culture. Similar effects were observed in these cell lines with the reference antimitotic chemotherapy paclitaxel (Table 1 and Fig. 1). We have shown that paclitaxel has a reducing effect on 4T1 cell viability in 2D culture compared to A549 (~five-fold lower) and HeLa (~ten-fold lower) cells, thus reflecting the resistance of 4T1 cells to paclitaxel. In addition, although 4T1-RFP spheroids were surprisingly more sensitive to low doses of paclitaxel than monolayer 4T1-RFP cells, high concentrations of paclitaxel failed to inhibit more than 50% of the cell proliferation of both A549 and 4T1 spheroids. Thus, PP-13 affected the proliferation of invasive cells *in vitro*, including those that are resistant to paclitaxel.

3.2. PP-13 treatment induces mitotic blockade in cancer cell spheroids

We previously demonstrated that PP-13 induced a transient mitotic blockade by interfering with mitotic spindle organization and microtubule dynamics in monolayer cell cultures [9].

Here, we analyzed the effect of PP-13 on mitosis in spheroids. The cell viability of HeLa-EGFP/RFP spheroids was not impacted by a short 24 h treatment of 200 nmol.L^{-1} PP-13 (data not shown). Alpha-tubulin and phosphorylated histone H3 (H3P), a marker of late G_2/M cell cycle phase, were analyzed by confocal microscopy on HeLa-EGFP/RFP spheroid sections (Fig. 2A). We observed that PP-13 led to mitotic defects, including multiple misoriented and shortened mitotic spindles (green arrows) associated with chromosomes miscongression (blue arrows). In addition, we showed a significant increase in the level of H3P after 24 h of PP-13 treatment, reflecting the strong accumulation of cells in mitosis in the HeLa-EGFP/RFP spheroids (Fig. 2C). As expected, paclitaxel also enhanced the level of H3P in HeLa-EGFP/RFP spheroids but to a lower extent than PP-13 and with an effect mainly on the cells at the periphery of the spheroids (Fig. 2B and 2C). Accumulation of H3P in response to PP-13 treatment was also increased in A549 spheroids compared to untreated control (Fig. 2C), and was confirmed by western blot of the three spheroid types (Fig. 2D). Finally, after 72 h of PP-13 treatment, the HeLa-EGFP/RFP spheroids showed a significant increase in cleaved caspase-3 (Fig. 2E and 2F). Therefore, in spheroid cultures, PP-13 induced mitotic spindle disorganization, mitotic blockade, inhibition of cell growth and apoptosis.

3.3. PP-13 inhibits angiogenesis in vitro

Because most of the microtubule-targeting agents also exhibit antiangiogenic properties [3, 6, 15, 16], we investigated the effects of PP-13 on capillary-like structure formation *in vitro* using HUVECs plated on a Matrigel basement membrane. In control conditions, endothelial cells aligned and formed organized networks of capillary-like structures after 6 h (Fig. 3A). PP-13 treatment reduced the total number of branching points, the number of loops, the length of the tubes, and the total cell-covered area compared to the control (Fig. 3B). Altogether, PP-

13 altered the ability of HUVECs to form tube-like structures. The concentrations of PP-13 that were used had limited impact on HUVEC proliferation (Fig. 3C). Hence, this suggested that PP-13 displayed antiangiogenic properties in vitro.

3.4. PP-13 inhibits the migration of cancer cells in vitro

Given the essential role of microtubules in cell motility, we investigated whether the PP-13 tubulin inhibitor impacted HeLa, A549, and 4T1-rvLuc2 cell migration and invasiveness in vitro. The impact of PP-13 on the motility of cells was examined using an in vitro wound-healing assay. We observed that PP-13 significantly reduced the motility of the three cell lines in a dose-dependent manner, and as paclitaxel (Fig. 4A and 4B). The effect of PP-13 on invasive migration was assessed with Matrigel in transwell chambers. PP-13 exerted a strong inhibitory effect on the invasion of the three cell lines (Fig. 4C and 4D). Paclitaxel also inhibited the invasion of these cells. These results indicated that PP-13 is able to slow down cell motility and invasion in vitro.

3.5. PP-13 inhibits the migration of cancer cells in vivo

We previously showed that PP-13 reduces tumor growth and metastatic invasion *in vivo* by using H358 NSCLC cells engrafted onto chicken chorioallantoic membranes (CAMs) [9]. Here, we used A549 NSCLC cells engrafted onto the CAMs to evaluate the efficacy of PP-13 on the migration of invasive cancer cells. The tumors were treated every other day with vehicle (control), PP-13, or paclitaxel (Fig. 5A). At the end of the experiment, the tumors were recovered from the upper CAMs and weighed. We used a very low concentration of PP-13 (0.13 µmol.L-1) compared to the > 10 µmol.L-1 PP-13 IC_{50} in the A549 spheroid cell

culture (Table 1), which did not inhibit A549 tumor growth (Fig. 5B). Analysis of the presence of A549 cells at the lower CAM by qPCR, allowing for the accurate detection of tumor cell dissemination, showed that this low dose of PP-13 significantly reduced the metastatic ability of A549 cells compared to the control (Fig. 5C). Paclitaxel was used as a positive control at a concentration known to inhibit A549 tumor growth and metastatic dissemination without inducing significant toxicity (Fig. 5B and 5C) [9]. These results suggested that PP-13 inhibited invasion in vivo. Furthermore, treatment with PP-13 did not significantly increase the mortality (two embryos died in the control group, and one embryo died in both paclitaxel and PP-13-treated groups) or abnormalities (no abnormality observed on surviving embryos for the different experimental groups) on chicken embryos, indicating that it was well tolerated.

3.6. PP-13 impairs tumor progression and metastasis in an allogeneic breast cancer model

To further evaluate the effect of PP-13 on tumor growth and metastasis formation, we used the allogeneic model of 4T1-rvLuc2 cell engraftment in the mammary fat pads of mice. We chose this model because once engrafted orthotopically in the mammary gland, 4T1-rvLuc2 mouse cancer cells metastasize to multiple distant sites (lymph nodes, lungs, liver, bone, brain), thus mimicking human breast cancers [17]. As soon as the 4T1-rvLuc2 cells were inoculated, the mice were randomly divided into four groups: one control group, one group treated with paclitaxel (0.5 $mg.kg^{-1}$) and two groups treated with PP-13 (0.5 and 1 $mg.kg^{-1}$) (Fig. 5D). The low concentrations of PP-13 were chosen based on the results obtained on chick embryo tumor model showing an inhibitory effect of PP-13 at very low dose, and were compared to the same concentration of the standard chemotherapy paclitaxel. Intraperitoneal

injections of each treatment were performed three times per week. The tumor progression was not affected at early time points, but the final tumor volumes were significantly lower after three weeks for the two groups treated with PP-13 in this rapidly progressing breast cancer model (Fig. 5E). The potential antiangiogenic activity of PP-13 in vivo was assessed sections performed on primary tumors stained with an anti-CD31 antibody. The microvessel density was counted and showed no significant difference between the treatments at the concentrations used and at this time-point (Fig. 5F). No significant difference between the treatments was observed in Ki67 immunostaining either (data not shown).

In vivo bioluminescence imaging was used to follow the development of thoracic metastases before and after primary tumor resection ~~(Fig. 5D)~~. Paclitaxel had no effect on the bioluminescence signal compared to the control treatment and even slightly enhanced it at day 28 (Fig. 6A and 6B). In contrast, the signal of thoracic metastasis was reduced with PP-13 treatment. Of note, both PP-13 and paclitaxel treatment reduced the number of mice with thoracic metastases compared to the control treatment from 2 weeks of treatment ~~(Fig. 6C)~~(Table 2). These results were confirmed by measuring bioluminescence in the lungs ex vivo at the end of the experiment (day 35) (Fig. 6C). This showed a non-significant 66% reduction in the lung metastasis signal in mice treated with 1 $mg.kg^{-1}$ PP-13 compared to control mice (Fig. 6D). In addition, ex vivo, the axillary and brachial lymph nodes showed a significant decrease in signal in both of the PP-13-treated groups compared to the control and paclitaxel-treated groups (Fig. 7A and 7B). The percentage of mice with axillary and brachial lymph node metastases was reduced in a dose-dependent manner in the PP-13-treated groups compared to the control and paclitaxel-treated groups ~~(Fig. 7C)~~(Table 2), as was the number of metastatic axillary and brachial lymph nodes (Fig. 7A). Taken together, these results

showed that PP-13 decreased tumor and metastatic ~~growth~~ dissemination in this breast cancer model.

3.7. PP-13 shows no adverse side effects in vivo

We assessed the toxicity of PP-13 and paclitaxel *in vivo*. There was no body-weight loss in the control and PP-13-treated mice over the course of the experiment, while mice exposed to paclitaxel displayed a significant decrease in body weight at the end of the experiment ~~(Fig. 7E)~~ (Table 3). In addition, one of the eight mice in each of the paclitaxel and control groups died before the end of the experiment probably because of tumor progression, while all PP-13-treated mice survived suggesting that PP-13 may control tumor progression.

We paid particular attention to some of the side effects described for conventional spindle poisons in patients. Serum biochemical analysis showed significant decreases in phosphorus, creatinine, and glucose in paclitaxel-treated mice compared to the control group (Table 4). No significant changes in serum biochemical values were reported in PP-13-treated mice, except a small and isolated decrease in blood urea nitrogen that did not reflect any renal toxicity in this context. In addition, macroscopic analyses of the organs of the treated mice did not show evidence of damage (data not shown). Hematological analysis of the blood and bone marrow cells from mice treated with PP-13 did not reveal any apparent signs of myelosuppression or other hematological abnormalities compared to the control (Table 5). In contrast, paclitaxel treatment led to a significant reduction in the white blood cell (WBC) count and a slight increase in the mean corpuscular hemoglobin concentration (MCHC).

Overall, these data suggest that PP-13 displays a favorable safety profile, as it slows both tumor and metastasis progression and is well tolerated at these doses compared to the control and paclitaxel.

4. Discussion

The new pyrrolo[2,3d]pyrimidine-based colchicine-binding site agent PP-13 showed promising anticancer properties *in vitro* [9]. In this study, we explored the therapeutic potential of PP-13, particularly in conditions leading to invasive cancer cell phenotype, and compared the effects of PP-13 with those of paclitaxel, a widely used tubulin-targeting agent in solid tumors. We showed that PP-13 inhibited proliferation, migration and angiogenesis in vitro, which may potentiate its antineoplastic activity, and reduced metastatic ~~progression~~ dissemination in paclitaxel-resistant tumors in vivo, with no detectable adverse side effects.

We confirmed the in vitro antitumor effects of PP-13 in spheroids. The PP-13-treated spheroids showed enhanced H3P levels associated with defects in mitotic spindle organization and chromosome congression, thus confirming in three-dimensions models that PP-13 induced an early mitotic blockade. Late caspase-3-dependent apoptotic mechanisms contributed to the decrease in spheroid growth, as was previously described in two-dimensions cell cultures [9]. Spheroids are currently considered to be a more suitable model than monolayer cell cultures because they better mimic the *in vivo* three-dimensions tumor environment and cell-cell and cell-extracellular matrix interactions [18-20]. Large spheroids (≥ 300 µm diameter), such as those generated in our experiments, display a hypoxic core resulting from chemical gradients of oxygen and nutrients that are correlated with chemoresistance, as reported in developing tumors [21]. We observed differences in the IC_{50} values of PP-13 between monolayer cell culture and spheroids. In particular, A549 cells were

resistant to PP-13 when cultured in spheroids, in contrast to monolayer cell culture, suggesting that the effect of PP-13 observed on two-dimensions-culture cell proliferation is reduced in spheroids. The presence of various environmental factors affecting the tumor development (e.g., cell–cell adhesion, cell-cycle distribution, local pH, extracellular matrix) [20] could explain the lower sensitivity of spheroid cancer cells to drugs compared to two-dimensions cell cultures, as was also observed in different in vivo tumor models [22-24]. The physicochemical properties of PP-13 could also be responsible for the lower sensitivity in three-dimensions cell culture.

Despite opposite mechanisms of action (microtubule stabilization or depolymerization) [3], both PP-13 and paclitaxel lead to the disruption of the microtubule organization and the induction of cancer cell cycle arrest and apoptosis.

Angiogenesis and cancer cell migration are attractive therapeutic targets [25]. The widely used capillary-like tube formation assay aids in studying the effects of new molecules on many steps of neoangiogenesis, including endothelial cell adhesion, migration, and tubule formation [26]. With this approach, we showed that PP-13 interfered with the tubule assembly in vitro by decreasing both the number of loops and branch nodes, the total length of the formed tubes and the cell-covered area. Using in vivo 4T1 primary breast tumor models, we did not observe any impact of PP-13 on microvessel density, suggesting that such PP-13 concentrations were inadequate to induce antiangiogenic activities and/or that the study time was not suitable to inhibit endothelial cells in vivo in this rapidly progressing breast cancer orthotopic model.

PP-13 inhibited cell motility and invasion both in vitro and in vivo. In vitro, we found that PP-13 inhibited cancer cell migration in the three metastatic tumor cell types. In addition, PP-13 reduced metastatic invasion in H358 [9] and A549 NSCLC cells engrafted onto chicken

CAMs at concentrations that did not inhibit cell proliferation in A549 spheroids. Accordingly, PP-13 did not inhibit A549 tumor growth in chicken CAMs. This confirmed the lower effect of PP-13 on cell proliferation in spheroids and in vivo compared to monolayer cell culture.

The orthotopic mouse model of breast cancer that was used is clinically relevant to predict the influence of the organ microenvironment on tumor cell behavior and to study the cancer cell invasion and metastatic growth [27]. Although PP-13 did not inhibit in vivo tumor cell migration and metastasis seeding at the concentrations used, we observed that the growth of the metastases was delayed, and their size remained small in both lungs and lymph nodes when the cells migrated from the primary tumor. Although PP-13 had both antiproliferative and antimigration effects in vitro, the in vivo experiments indicated that the effect of the drug on the inhibition of invasion was stronger than its antiproliferative effects.

Overall, our data indicate that PP-13 could be a potent agent to decrease the growth of both primary tumors and their metastases, especially for triple-negative breast cancers (TNBC), which account for nearly 15% of breast cancers and have poor therapeutic options and prognoses [28]. The 4T1 allogeneic transplant mouse model mimics TNBC in humans and is associated with a high propensity to metastasize, primarily in the lymph nodes and lungs. The therapeutic arsenal for TNBC mainly consists of anthracyclines and taxane-based chemotherapies; however, the emergence of resistance and frequent tumor recurrence support the need to identify alternative drugs for the management of refractory tumors. The 4T1 model thus represents an interesting approach to screen new molecules for TNBC therapy, especially since it spontaneously metastasizes in the same regions as in TNBC and easily develops resistance to chemotherapies classically used in TNBC [29, 30]. Compared to paclitaxel, which was used as a reference treatment to reduce metastasis while limiting the

adverse effects, PP-13 moderately inhibited primary tumor growth and delayed metastatic growth.

PP-13 treatment did not show any sign of toxicity compared to the controls; there was notably an absence of myelosuppression, which is classically observed with conventional antimitotic drug treatments or colchicine binding-site agents [3]. At the same dose, paclitaxel led to a significant decrease in white blood cell count, as has been previously reported [31], as well as a slight reduction in plasma glycaemia, phosphorus and creatinine and an increase in MCHC. Further investigations with higher concentrations of PP-13 will be needed to establish the maximal antitumor effect of PP-13, ~~and~~ the therapeutic index of the molecule, and long-term survival. In addition, PP-13 has no kinase activity [9] but may target other molecule than tubulin, that remains to determine.

~~5. Conclusions~~

In summary, PP-13 significantly reduced the cancer cell migration and neoangiogenesis processes in vitro. PP-13 also led to a reduction in both tumor growth and metastatic ~~progression~~ dissemination in vivo in a mouse orthotopic TNBC model without any significant toxicity. These findings suggest that PP-13 should be an efficient anticancer therapy and an *alternative* option to conventional spindle poisons such as taxanes or vinca-alkaloids.

5. Acknowledgements

We acknowledge the assistance of Alexeï Grichine, Mylène Pezet and Jacques Mazzega (Optical Microscopy Platform - Cell Imaging, INSERM U1209). We kindly thank Dr. Lucie Sancey for critical evaluation of the data, and Lilya Mediouni for her help. This work was

supported by the Institut Curie, the CNRS, the INSERM, and grants from “La Fondation de France” and “La Ligue contre le Cancer (comité de l’Isère)”. The *in vivo* evaluation was performed by the OPTIMAL facility, which is part of the France Live Imaging Program (FLI-Grenoble; French program “Investissement d’Avenir”; grant “Infrastructure d’avenir en Biologie Santé,” ANR-11-INBS-0006).

6. Author contributions

PG, BB, and AH conceived the project, designed the experiments, and interpreted the data. PG, LL, MC, LV, MH, and JV were involved in acquisition, analysis and interpretation of the data. VB, MW, and AO managed automated quantifications. VJ, MH, and JV designed the *in vivo* experiment. FMB synthesized and characterized PP-13. JLC, BB and AH supervised the research and analyses. PG, BB and AH supervised the whole project and wrote the manuscript. All authors reviewed the manuscript.

7. References

[1] K.D. Miller, R.L. Siegel, C.C. Lin, A.B. Mariotto, J.L. Kramer, J.H. Rowland, et al., Cancer treatment and survivorship statistics, 2016, CA Cancer J Clin 66(4) 2016: 271-89.

[2] M.A. Jordan, L. Wilson, Microtubules as a target for anticancer drugs, Nat Rev Cancer 4(4) 2004: 253-65.

[3] C. Dumontet, M.A. Jordan, Microtubule-binding agents: a dynamic field of cancer therapeutics, Nat Rev Drug Discov 9(10) 2010: 790-803.

[4] M.A. Jordan, Mechanism of action of antitumor drugs that interact with microtubules and tubulin, Curr Med Chem Anticancer Agents 2(1) 2002: 1-17.

[5] D. Fanale, G. Bronte, F. Passiglia, V. Calo, M. Castiglia, F. Di Piazza, et al., Stabilizing versus destabilizing the microtubules: a double-edge sword for an effective cancer treatment option?, Anal Cell Pathol (Amst) 2015 2015: 690916.

[6] E.L. Schwartz, Antivascular actions of microtubule-binding drugs, Clin Cancer Res 15(8) 2009: 2594-601.

[7] C. Kanthou, G.M. Tozer, Microtubule depolymerizing vascular disrupting agents: novel therapeutic agents for oncology and other pathologies, Int J Exp Pathol 90(3) 2009: 284-94.

[8] D. Bates, A. Eastman, Microtubule destabilising agents: far more than just antimitotic anticancer drugs, Br J Clin Pharmacol 83(2) 2017: 255-268.

[9] P. Gilson, J.F. Josa-Prado, C. Beauvineau, D. Naud-Martin, L. Vanwontherghem, F. Mahuteau-Betzer, et al., Identification of pyrrolopyrimidin derivative PP-13 as a novel microtubule-destabilizing agent with promising anticancer properties, Scientific Reports 7 2017: 10209.

[10] P. Steigemann, C. Wurzenberger, M.H. Schmitz, M. Held, J. Guizetti, S. Maar, et al., Aurora B-mediated abscission checkpoint protects against tetraploidization, Cell 136(3) 2009: 473-84.

[11] B. Busser, L. Sancey, V. Josserand, C. Niang, M.C. Favrot, J.L. Coll, et al., Amphiregulin promotes BAX inhibition and resistance to gefitinib in non-small-cell lung cancers, Molecular therapy 18(3) 2010: 528-35.

[12] Q. Zheng, B.K. Milthorpe, A.S. Jones, Direct neural network application for automated cell recognition, Cytometry A 57(1) 2004: 1-9.

[13] B. Busser, L. Sancey, V. Josserand, C. Niang, S. Khochbin, M.C. Favrot, et al., Amphiregulin promotes resistance to gefitinib in nonsmall cell lung cancer cells by regulating Ku70 acetylation, Molecular therapy 18(3) 2010: 536-43.

[14] V. Jeannot, S. Mazzaferro, J. Lavaud, L. Vanwonterghem, M. Henry, M. Arboleas, et al., Targeting CD44 receptor-positive lung tumors using polysaccharide-based nanocarriers: Influence of nanoparticle size and administration route, Nanomedicine 12(4) 2016: 921-32.

[15] E. Pasquier, S. Honore, D. Braguer, Microtubule-targeting agents in angiogenesis: where do we stand?, Drug Resist Updat 9(1-2) 2006: 74-86.

[16] E. Pasquier, N. Andre, D. Braguer, Targeting microtubules to inhibit angiogenesis and disrupt tumour vasculature: implications for cancer treatment, Curr Cancer Drug Targets 7(6) 2007: 566-81.

[17] B.A. Pulaski, S. Ostrand-Rosenberg, Mouse 4T1 breast tumor model, Curr Protoc Immunol Chapter 20 2001: Unit 20 2.

[18] C.J. Lovitt, T.B. Shelper, V.M. Avery, Advanced cell culture techniques for cancer drug discovery, Biology (Basel) 3(2) 2014: 345-67.

[19] F. Hirschhaeuser, H. Menne, C. Dittfeld, J. West, W. Mueller-Klieser, L.A. Kunz-Schughart, Multicellular tumor spheroids: an underestimated tool is catching up again, Journal of biotechnology 148(1) 2010: 3-15.

[20] G. Mehta, A.Y. Hsiao, M. Ingram, G.D. Luker, S. Takayama, Opportunities and challenges for use of tumor spheroids as models to test drug delivery and efficacy, Journal of controlled release : official journal of the Controlled Release Society 164(2) 2012: 192-204.

[21] S. Daster, N. Amatruda, D. Calabrese, R. Ivanek, E. Turrini, R.A. Droeser, et al., Induction of hypoxia and necrosis in multicellular tumor spheroids is associated with resistance to chemotherapy treatment, Oncotarget 8(1) 2017: 1725-1736.

[22] R. Edmondson, J.J. Broglie, A.F. Adcock, L. Yang, Three-dimensional cell culture systems and their applications in drug discovery and cell-based biosensors, Assay Drug Dev Technol 12(4) 2014: 207-18.

[23] S. Breslin, L. O'Driscoll, The relevance of using 3D cell cultures, in addition to 2D monolayer cultures, when evaluating breast cancer drug sensitivity and resistance, Oncotarget 7(29) 2016: 45745-45756.

[24] V.S. Nirmalanandhan, A. Duren, P. Hendricks, G. Vielhauer, G.S. Sittampalam, Activity of anticancer agents in a three-dimensional cell culture model, Assay Drug Dev Technol 8(5) 2010: 581-90.

[25] D. Hanahan, R.A. Weinberg, Hallmarks of cancer: the next generation, Cell 144(5) 2011: 646-74.

[26] D. Xie, D. Ju, C. Speyer, D. Gorski, M.A. Kosir, Strategic Endothelial Cell Tube Formation Assay: Comparing Extracellular Matrix and Growth Factor Reduced Extracellular Matrix, J Vis Exp (114) 2016.

[27] S. Man, R. Munoz, R.S. Kerbel, On the development of models in mice of advanced visceral metastatic disease for anti-cancer drug testing, Cancer Metastasis Rev 26(3-4) 2007: 737-47.

[28] P. Kaur, G.M. Nagaraja, H. Zheng, D. Gizachew, M. Galukande, S. Krishnan, et al., A mouse model for triple-negative breast cancer tumor-initiating cells (TNBC-TICs) exhibits similar aggressive phenotype to the human disease, BMC Cancer 12 2012: 120.

[29] L. Bao, A. Haque, K. Jackson, S. Hazari, K. Moroz, R. Jetly, et al., Increased expression of P-glycoprotein is associated with doxorubicin chemoresistance in the metastatic 4T1 breast cancer model, Am J Pathol 178(2) 2011: 838-52.

[30] T. Luo, J. Wang, Y. Yin, H. Hua, J. Jing, X. Sun, et al., (-)-Epigallocatechin gallate sensitizes breast cancer cells to paclitaxel in a murine model of breast carcinoma, Breast Cancer Res 12(1) 2010: R8.

[31] E.A. Perez, Paclitaxel in Breast Cancer, Oncologist 3(6) 1998: 373-389.

Figure legends

Table 1: Sensitivity of cancer cell lines to PP-13 and paclitaxel. The drug concentrations required to inhibit cell growth by 50% (IC_{50}) at 72h in HeLa cells, HeLa mEGFP-α-tubulin and mRFP-H2B cells (HeLa-EGFP/RFP), A549 cells, 4T1 mRFP-H2B cells (4T1-RFP) and 4T1-rvLuc2 cells cultured in 2D-monolayer (2D) or spheroids. Data represent the mean ± SD of three independent experiments, each performed in triplicate.

Table 2: PP-13 decreased the number of mice with thoracic and lymph node metastases. Mice with 4T1-rvLuc2 tumors were treated with vehicle (control), paclitaxel 0.5 $mg.kg^{-1}$, or PP-13 (0.5 and 1 $mg.kg^{-1}$) (see Fig. 5D). Number and percentages of mice with thoracic metastases at day 14, and with invaded axillary and brachial lymph nodes at day 35 are shown in each group.

Table 3: Mice body-weight. Mice with 4T1-rvLuc2 tumors were treated with vehicle (control), paclitaxel 0.5 $mg.kg^{-1}$, or PP-13 (0.5 and 1 $mg.kg^{-1}$) (see Fig. 5D). Mice body-weight is expressed as mean ± SEM (n=8, except in paclitaxel-treated group at day 35, n=7), and as percentage of initial body-weight (day 0). * p <0.05; two-way ANOVA with Bonferroni post-test (day 35 compared to day 28).

Table 4: Biochemical analyses of mice. Plasma biochemical values of mice after control, paclitaxel or PP-13 treatments were assessed. Data represent the mean ± SD of 6 mice per group. Data were analyzed using Mann-Whitney *U*-test. * Significant as compared to control group.

Table 5: Hematological and bone marrows analyses of mice. Complete blood count and white blood cells count and evaluation of the global cell abundance and megakaryocyte and leukocyte counts in the bone marrow, from mice treated with control, paclitaxel, or PP-13. Data represent the mean ± SD of 8 mice per group. # from score 1 (low abundance) to score 4 (high abundance). Data were analyzed using one-way analysis of variance. NS: not significant.

Figure 1: Viability of cancer cells treated with PP-13 or paclitaxel.

A. A549, 4T1 mRFP-H2B (4T1-RFP), and HeLa mEGFP-α-tubulin mRFP-H2B (HeLa-EGFP/RFP) were cultured in two-dimensions (2D) or in spheroids, and treated for 72 h with increasing concentrations of PP-13 (left) or paclitaxel (right), and the cell viability was assessed. Data represent the mean ± SD from three independent experiments, each performed in triplicate. **B.** Representative images of treated spheroids are shown. Bars: 100 µm.

Figure 2: Effects of PP-13 on cancer cell spheroids.

HeLa mEGFP-α-tubulin mRFP-H2B (HeLa-EGFP/RFP) spheroids were treated with vehicle (control), 200 nmol.L^{-1} PP-13, or 15 nmol.L^{-1} paclitaxel for 24 h (**A-D**) or for 72 h (**E-F**). A549 spheroids were treated for 24 h with vehicle (control) or 10 µmol.L^{-1} PP-13 (**C-D**). 4T1 mRFP-H2B (4T1-RFP) spheroids were treated for 24 h with vehicle (control) or 200 nmol.L^{-1} PP-13 (**D**). **A.** Representative confocal microscopy images of microtubules (α-tubulin-EGFP) and phosphorylated histone H3 (H3P, a marker of late G_2/M cell cycle phase) immunodetection in spheroid sections treated with vehicle (control) or PP-13. In purple: H3P, in green: α-tubulin, in red: H2B-RFP, in blue: Hoechst-stained nuclei. The green and blue arrows indicate multipolar mitotic spindles and miscongressed chromosomes, respectively. Scale bars: 50 µm (20x magnification) and 10 µm (63x magnification). **B.** Representative

confocal microscopy images of H3P analyzed by immunofluorescence on spheroids sections treated with vehicle (control), or paclitaxel. In pink: H3P, in blue: Hoechst-stained nuclei. Scale bars: 50 µm. **C.** The percentage of H3P was calculated as the number of H3P-positive cells in control (n = 7, HeLa-EGFP/RFP; n=11, A549), PP-13 (n = 13, HeLa-EGFP/RFP; n=11, A549), or paclitaxel (n = 9, HeLa-EGFP/RFP) spheroids, with two or three sections per spheroid. Data are expressed as the mean ± SD. *** $p < 0.0001$ between control and treated conditions; Mann-Whitney *U*-test. **D.** Western blot analysis of H3P in A549, 4T1-RFP, or HeLa-EGFP/RFP pooled spheroids (n = 10 spheroids in each condition). Actin was used as a loading control. Values indicate relative H3P/actin ratio. **E.** Representative confocal microscopy images of cleaved caspase-3 immunodetection in spheroid sections. In purple: cleaved caspase-3, in green: α-tubulin, in red: H2B-RFP, in blue: Hoechst-stained nuclei. Scale bars: 50 µm. **F.** Quantification of cleaved caspase-3 in spheroids (control, n = 9 spheroids; PP-13, n = 7 spheroids; with two or three sections per spheroids). Data are expressed as the mean ± SD. *** $p < 0.0001$ between control and treated conditions; Mann-Whitney *U*-test.

Figure 3: In vitro effects of PP-13 on angiogenesis.

HUVECs were treated with vehicle (control) or increasing concentrations of PP-13, as indicated, for 6 h. **A.** Capillary-like tube formation assay: representative images of the HUVEC capillary-like tube formation in each condition. Bar: 200 µm. **B.** Quantification of the tube length, the cell-covered area, the number of loops and the number of branching points. Data are expressed as the mean ± SD and as the percentages of vehicle condition to control the seeding variations between the experiments (n = 5). * $p < 0.05$; ** $p < 0.01$; *** $p < 0.001$ between control and treated conditions; Kruskal-Wallis test with Dunn's multiple

comparisons post hoc test. **C.** HUVEC cell viability was assessed. Data represent the mean ± SD ($n \geq 3$).

Figure 4: In vitro effects of PP-13 on cancer cell migration and invasion.

A-B. Wound-healing assay in A549, HeLa, and 4T1-rvLuc2 cells treated with vehicle (control) or increasing concentrations of PP-13 or paclitaxel for 12 h. **A.** Representative images from wound-healing assay experiment at 0 h and 12 h. Cells were treated with vehicle (control), 1 $\mu mol.L^{-1}$ (A549 and HeLa) or 0.5 $\mu mol.L^{-1}$ (4T1-rvLuc2) PP-13, 20 $nmol.L^{-1}$ (HeLa) or 50 $nmol.L^{-1}$ (A549) or 200 $nmol.L^{-1}$ (4T1-rvLuc2) paclitaxel. The white lane delineates the edges of the wound. **B.** Relative wound density over time in cells treated as indicated. The relative wound density at 0 h is arbitrarily set to 0%. Data are expressed as the mean ± SD. Experiments were performed at least five times in triplicate. * $p < 0.05$; ** $p < 0.01$; *** $p < 0.001$ compared to control or treated conditions as indicated; Friedman test with Dunn's multiple comparisons post hoc test. **C-D.** Matrigel invasion assay of A549, 4T1-rvLuc2 and HeLa cells treated treated with vehicle (control), 200 $nmol.L^{-1}$ (4T1-rvLuc2) or 500 $nmol.L^{-1}$ (A549, HeLa) PP-13, or 20 $nmol.L^{-1}$ (HeLa), 40 $nmol.L^{-1}$ (A549), or 150 $nmol.L^{-1}$ (4T1-rvLuc2) paclitaxel for 24 h. **C.** Representative images from methylen-blue stained cells treated with vehicle (control), PP-13, or paclitaxel. The red squares show the quantified cells. **D.** Quantification of invasion of cells treated with vehicle (control), PP-13, or paclitaxel. Cells were counted in ten fields per condition and in three independent experiments. Data are expressed as the mean ± SD and as the percentages of vehicle condition to control variations between the experiments. * $p < 0.05$; ** $p < 0.01$ between control and treated conditions; Mann-Whitney *U*-test.

Figure 5: Effects of PP-13 in vivo.

A. Schematic representation of the *in ovo* assay principle. A549 cells were engrafted onto chick embryo chorioallantoic membranes (CAMs) at E9, were randomized into three groups, and treatments with 0.5% DMSO (control, n = 18), 50 $\mu mol.L^{-1}$ paclitaxel (positive control of tumor growth inhibition, n = 17), or 0.13 $\mu mol.L^{-1}$ PP-13 (low dose, n = 18) were administered every other day for 10 days. **B.** Tumors were excised and weighted at the end of the treatments. The histogram represents the effect of treatments on A549 tumor weight (means ± SEM, n = 16). *** $p < 0.001$ compared to control; Kruskal-Wallis test. **C.** The presence of A549 cells in the lower CAM at the end of the experiment was evaluated by qPCR in ten random embryos per group. The histogram represents the effect of treatments on A549 metastases in the lower CAM (means ± SEM, n = 10). The relative amount of metastases in the lower CAM in the control group is arbitrarily set to one to control interindividual variations. *** $p < 0.001$ compared to control; Kruskal-Wallis test.

D. Schematic representation of orthotopic breast tumors and metastatic growth and of the treatment plan. The mice were inoculated with 4T1-rvLuc2 cells and randomized into four groups of eight mice. Vehicle (control), 0.5 $mg.kg^{-1}$ paclitaxel, or 0.5 or 1 $mg.kg^{-1}$ PP-13 were administered intraperitoneally three times a week. Thoracic bioluminescence imaging was performed once a week for five weeks. After three weeks, the primary tumors were resected. **E.** Primary tumor volume. Data represent the mean ± SEM in each group (n = 8). *** $p < 0.001$ compared to control group; two-way ANOVA with Bonferroni post hoc test. **F.** Histogram shows the CD31 positive staining quantification on frozen 4T1-tumor sections, expressed as the mean ± SD. The CD31 levels were determined after counting positive stained blood vessel area as described in methods, in three sections per tumor and in three tumors per group.

Figure 6: Effects of PP-13 on thoracic metastases in orthotopic breast tumor model.

Mice with 4T1-rvLuc2 tumors were treated with vehicle (control), paclitaxel 0.5 $mg.kg^{-1}$, or PP-13 (0.5 and 1 $mg.kg^{-1}$), 3 times a week (see Fig. 5D). **A.** *In vivo* bioluminescence images of the thoracic metastases (ventral view) in one representative mouse per group at day twenty-eight. **B.** Overtime quantification of *in vivo* bioluminescence signal in thoracic areas over the duration of the experiment (ventral and dorsal views). Data are expressed as the mean ± SEM (n = 8). * $p < 0.05$; **** $p < 0.0001$ compared to control or to paclitaxel-treated groups; two-way ANOVA with Bonferroni post hoc test. **C.** ~~Percentage of mice with and without thoracic metastases at day 14 in each group (n = 8). Numbers indicate the reduction in mice with lung metastases in each treatment group, compared to control group.~~ **~~D.~~** Ex vivo bioluminescence images of lungs at the end of the experiment (day 35). (n = 8, except in paclitaxel-treated group, n = 7). **~~E~~ D.** E*x vivo* bioluminescence signal in each lung at the end of the experiment (day 35). Bars: mean bioluminescence signal (n = 8, except in paclitaxel-treated group, n = 7). Number indicates the reduction (%) in mean bioluminescence signal in 1 $mg.kg^{-1}$ PP-13-treated group, compared to control group.

Figure 7: Effects of PP-13 on lymph node metastases.

Axillary and brachial lymph nodes were collected at the end of the experiment (day thirty-five) in 4T1-rvLuc2 mice treated as indicated. **A**. *Ex vivo* bioluminescence images of lymph nodes. RA, right axillary lymph node; LA, left axillary lymph node; RB, right brachial lymph node; LB, left brachial lymph node. Each line shows the lymph nodes of one mouse (n = 8, except in paclitaxel-treated group, n = 7). Numbers indicates the invaded lymph nodes and their percentages in each group. **B.** Ex vivo bioluminescence signal in each lymph node. Bars: median bioluminescence signal (n = 32 lymph nodes/group, 8 mice/group except in paclitaxel-treated group: 7 mice, 28 lymph nodes). * $p < 0.05$; *** $p < 0.001$; **** $p < 0.0001$

compared to control or treated groups; Kruskal-Wallis with Dunn's multiple comparisons post hoc test. ns, not significant. ~~**C.** Percentage of mice with and without invaded lymph nodes in each group (n = 8, except in paclitaxel-treated group, n = 7). Numbers indicate the reduction in mice with lymph node metastases in each treatment group compared to the control group. **D.** Percentage of lymph nodes with and without metastases in each group (n = 32, except in paclitaxel-treated group, n = 28). Numbers indicate the reduction in invaded lymph nodes in each treatment group compared to the control group. **E.** Mice body-weight (means ± SEM, n=8 except in paclitaxel-treated group at day 35, n = 7). * $p<0.05$; two-way ANOVA with Bonferroni post-tests; NS not significant.~~

The pyrrolopyrimidine colchicine-binding site agent PP-13 reduces the metastatic dissemination of invasive cancer cells in vitro and in vivo

Pauline Gilson[1,2,#], Morgane Couvet[1], Laetitia Vanwonterghem[1], Maxime Henry[1], Julien Vollaire[1], Vladimir Baulin[3], Marco Werner[3], Anna Orlowska[3], Véronique Josserand[1], Florence Mahuteau-Betzer[4], Laurence Lafanechère[5], Jean-Luc Coll[1], Benoit Busser[1,2,*], Amandine Hurbin[1,*]

[1] Cancer Target and Experimental Therapeutics, Institute for Advanced Biosciences, INSERM U1209, CNRS UMR5309, Grenoble Alpes University, Grenoble, France.

[2] Biochemistry Department, Grenoble University Hospital, Grenoble, France.

[3] Departament d'Enginyeria Quımica, Universitat Rovira i Virgili, Tarragona, Spain.

[4] Institut Curie, PSL Research University, CNRS, INSERM UMR9187/U1196, Orsay, France.

[5] Regulation and Pharmacology of the Cytoskeleton, Institute for Advanced Biosciences, INSERM U1209, CNRS UMR5309, Grenoble Alpes University, Grenoble, France.

[#] Present address: Université de Lorraine, Faculté de Pharmacie; CNRS UMR7039 CRAN, Nancy, France; and Institut de Cancérologie de Lorraine, Service de Biopathologie, Vandoeuvre-lès-Nancy, France.

[*] Co-last authors.

Corresponding authors:

Amandine Hurbin, Institute for Advanced Biosciences, INSERM U1209, CNRS UMR5309, Grenoble Alpes University, Grenoble, France. Tel: +33 4 76 54 95 53. Fax: +33 4 76 54 94 13. amandine.hurbin@inserm.fr.

Benoit Busser, Institute for Advanced Biosciences, INSERM U1209, CNRS UMR5309, Grenoble Alpes University, Grenoble, France. Tel: +33 4 76 54 94 20. Fax: +33 4 76 54 94 13. bbusser@chu-grenoble.fr.

Conflict of interest: The authors have no conflict of interest to declare.

Abstract

Standard chemotherapies that interfere with microtubule dynamics are a chemotherapeutic option used for the patients with advanced malignancies that invariably relapse after targeted therapies. However, major efforts are needed to reduce their toxicity, optimize their efficacy, and reduce cancer chemoresistance to these agents. We previously identified a pyrrolo[2,3d]pyrimidine-based microtubule-depolymerizing agent (PP-13) that binds to the colchicine site of β-tubulin and exhibits anticancer properties in solid human cancer cells, including chemoresistant subtypes. Here, we investigated the therapeutic potential of PP-13 in vitro and in vivo. PP-13 induced a mitotic blockade and apoptosis in several cancer cells cultured in two-dimensions or three-dimensions spheroids, in conjunction with reduced cell proliferation. Capillary-like tube formation assays using HUVECs showed that PP-13 displayed antiangiogenic properties. It also inhibited cancer cell motility and invasion, in in vitro wound-healing and transwell migration assays. Low concentration PP-13 (130 $nmol.L^{-1}$) treatment significantly reduced the metastatic invasiveness of human cancer cells engrafts on chicken chorioallantoic membrane. In nude mice, 0.5 or 1 $mg.kg^{-1}$ PP-13 intraperitoneally administered three-times a week reduced the sizes of paclitaxel-refractory orthotopic breast tumors, delayed the progression of metastasis, and decreased the global metastatic load compared to 0.5 $mg.kg^{-1}$ paclitaxel or vehicle alone. PP-13 did not show any apparent early adverse effect in vivo. These data suggest that PP-13 is a promising alternative to standard chemotherapy in antimitotic drug-refractory tumors, especially through its impact on metastasis.

Keywords: spheroids, invasion, metastasis, paclitaxel, drug-refractory tumors, pyrrolopyrimidine

1. Introduction

Despite recent innovations in targeted anticancer strategies over the last decade, non-selective chemotherapies are still widely used for the clinical management of various patients with advanced malignancies [1]. Microtubules represent one of the most common targets for chemotherapies, as they are crucial for the maintenance of cell shape, intracellular transport, cell motility, and chromosome migration during cell division [2]. Taxanes and vinca-alkaloids are the two main classes of microtubule-targeting agents and are classically known to induce microtubule stabilization and depolymerization, respectively [3]. Therapeutic doses of all compounds from these two families lead to the alteration of the dynamic state of the microtubules, which ultimately induces multipolar divisions and causes cell death [4, 5]. Beyond their cytotoxic activity, most microtubule-binding agents display antimetastatic, antiangiogenic or vascular-disrupting properties, supporting their use as therapeutic agents for cancer treatment [6-8]. However, the troublesome side effects of microtubule inhibitors, particularly myelosuppression and peripheral neurotoxicity, and the emergence of chemoresistance, predominantly from the overexpression of efflux transporters, drastically limits their therapeutic outcomes [3], hence underscoring the need for alternative agents.

We recently identified a novel pyrrolopyrimidine-based microtubule-depolymerizing agent (PP-13) that was effective in vitro on a wide range of human cancer cells [9]. PP-13 has no kinase activity, directly binds to the colchicine binding site of β-tubulin, interferes with microtubule organization and induces spindle multipolarity, transient mitotic cell cycle arrest and apoptosis [9]. Interestingly, in marked contrast to conventional microtubule-damaging drugs, PP-13 escapes resistance mechanisms linked to the presence of efflux pumps, which underlies its *potential* anticancer activity for multidrug-resistant cancer cells [9].

Based on the efficacy of PP-13 against human cancer cell proliferation and multidrug-resistant cancer cells, the aim of the present study was to investigate the therapeutic potential of PP-13 against highly invasive and aggressive cancer cell lines in vitro and in vivo. The effects of PP-13 were analyzed in HeLa cervical cancer cells, A549 NSCLC cells and 4T1 murine mammary cancer cells that were cultured in two-dimensions monolayers or in three-dimensions-spheroids. The impact of PP-13 on cell migration, metastasis and angiogenesis was evaluated. Since no colchicine binding-site agent is currently used in clinic for cancer treatment, we assessed the clinical potential of PP-13 activity in comparison with paclitaxel, a standard anti-mitotic chemotherapy that is routinely used for the treatment of a wide range of solid cancers, and is considered a reference treatment for in vitro and in vivo studies of new microtubule-targeting agents.

2. Material and Methods

2.1. Materials

Paclitaxel was obtained from Sigma-Aldrich (Saint-Quentin-Fallavier, France). PP-13 was obtained from Institut Curie (CNRS Chemical library, 2004 version), as described in [9]. All drugs were dissolved in sterile anhydrous dimethyl sulfoxide (DMSO, Carl Roth, Karlsruhe, Germany) at a 10 $mmol.L^{-1}$ stock solution. Phospho-histone H3 (H3P), and active caspase-3 antibodies were purchased from Cell Signaling Technology (Ozyme, Saint-Quentin-Les-Yvelines, France), and conjugated Alexa Fluor 633 goat anti-rabbit antibodies were from Thermo Fisher Scientific (Saint-Aubin, France).

2.2. Cell lines and culture

The human HeLa and A549 cell lines and the murine 4T1 cells were obtained from the American Type Culture Collection (ATCC, Manassas, VA, USA). HeLa cells expressing mEGFP-α-tubulin and mRFP-H2B (HeLa-EGFP/RFP) were a generous gift from Dr. D. Gerlich [10]. The 4T1 cells were stably transfected with a plasmid expressing the fusion histone H2B-RFP (provided by Dr. C. Albigès-Rizo, Institute for Advanced Biosciences, Grenoble, France) (4T1-RFP) or with the pGL4.50[*luc2*/CMV/Hygro] vector encoding the firefly luciferase reporter gene *luc2* (Promega, Charbonnière, France) (4T1-rvLuc2) using JetPEI (Polyplus Transfection, Illkirch, France) according to the manufacturer's protocol. Transfected cells were selected with G418 antibiotic (Invivogen Europe, Toulouse, France, ant-gn-5) and amplified. All cells were routinely tested for the presence of mycoplasma (MYCOALERT® Mycoplasma Detection Kit, Lonza, Amboise, France) and used within three months after thawing. A549, HeLa, and HeLa-EGFP/RFP cell lines were authenticated by DNA STR profiling (ATCC Cell line Authentication Service, Manassas, VA, USA). Human umbilical vein endothelial cells (HUVECs, passage two to five; Lonza) were cultured in complete medium of the EGM-2 BulletKit (Lonza, Amboise, France).

2.2.1. Two-dimensions (2D) cell culture

Cells were maintained in culture at 37°C in the appropriate medium with 10% FBS in a 5% CO_2 humidified atmosphere, and the cell morphology was routinely checked.

2.2.2. Three-dimensions (3D) cell culture

Spheroids were generated by plating A549 (4000 cells/well), HeLa-EGFP/RFP (1000 cells/well), or 4T1-RFP (2000 cells/well) cells into 96-well round bottom ultra-low attachment (ULA) spheroid microplates (Corning, Tewksbury, MA, USA). The spheroid

culture was performed in medium with 10% FBS in a humidified atmosphere with 5% CO_2. Spheroid formation and growth were assessed by microscopic examination using an inverted microscope and by imaging the spheroids at each time point.

2.3. In vitro cytotoxicity assays

Cell proliferation assays were conducted in 96-well culture plates. 2D-cultured cells and spheroids were cultured for 24 h and 72 h, respectively, prior to treatment with PP-13 or paclitaxel in medium containing 10% FBS for 72 h. The cell viability was quantified using CELLTITER 96® AQueous One Solution cell proliferation assay (Promega, Charbonnière, France) in 2D cell models or by using the CELLTITER-GLO® 3D Cell Viability Assay (Promega, Charbonnière, France) in spheroids. The drug concentrations required to inhibit cell growth by 50% (IC_{50}) were interpolated from the dose-response curves.

2.4. Immunofluorescence analyses of spheroids

After PP-13 treatment, the spheroids were washed, fixed overnight at 4°C in 4% paraformaldehyde, and then washed, frozen and cut into 7-µm sections before mounting onto SuperFrost UltraPlus slides (Thermo Fisher Scientific, Saint-Aubin, France). Cryosections were rehydrated in PBS-glycine, permeabilized for 1 h in PBS with 2% Triton X-100, washed in PBS-glycine, blocked in 10% goat serum and incubated overnight at 4°C with primary antibodies. The sections were then washed in 0.2% Tween-20/PBS and incubated for 1 h with conjugated secondary antibodies. Hoechst was used to counterstain the cell nuclei.

Fluorescence microscopy was carried out using a confocal microscope (LSM 710; Carl Zeiss, Jena, Germany). An objective Plan Apochromat 20×/0.8 NA in air and an objective Plan

Apochromat 63×/1.4 NA in oil were used. The H3P and active caspase-3 expression levels in spheroids were counted based on color thresholding image adjustment using ImageJ software (NIH, Bethesda, MD, USA) and the images were blinded. The percentage of H3P was calculated as the number of H3P-positive cells in control and PP-13-treated spheroids ($n \geq 7$ as indicated in the figure legends, with three different sections analyzed per spheroid). The percentage of cleaved caspase-3 was calculated as the number of cleaved caspase-3-positive cells in control and treated spheroids ($n \geq 7$ as indicated in the figure legends, with two or three different sections analyzed per spheroid).

2.5. Immunoblotting

Western blot analyses were performed as previously described [11] after protein extraction of ten pooled spheroids per condition and sonication. H3P and actin intensities were quantified using the Image J software and the relative densitometric area for H3P were determined according to actin signal in each condition.

2.6. Wound-healing assay

A549, 4T1-rvLuc2 and HeLa cells were seeded into 96-well plates (15000 cells/well) and allowed to grow for 24 h until confluence. Scratching the surface with a wound maker physically wounded the cell monolayers, and increasing concentrations of PP-13 or DMSO were added into the medium. Images of the cells invading the scratch wound were monitored for 12 h using the IncuCyte S3 Live-Cell analysis system (Essen Bioscience, Hertfordshire, UK). The relative wound density was analyzed using the IncuCyte S3 software.

2.7. Transwell migration and invasion assays

A549, 4T1-rvLuc2 and HeLa cells were plated (75000 cells) on top of a transwell chamber with Matrigel (Corning, Tewksbury, MA, USA) under starvation conditions, and complete medium was added into the well. After 24 h of incubation with PP-13 or DMSO, cells that reached the bottom of the transwell were stained with methylene blue and observed by microscopy (AxioImager M2, Carl Zeiss, Jena, Germany). Ten images were obtained per condition and were blinded for quantification. Cell invasion was quantified using a fully connected, three-layer back-propagation neuronal network, as previously described [12]. Briefly, the input layer of the network was prepared to receive 12 9 12 pixel images, with three-color channels totaling up to 12 9 12 9 3 input neurons. A total of twenty-four neurons in the hidden layer were utilized. The output layer consists of two neurons corresponding to the two classes E (empty space between structures) and S (structure) with respect to which each pixel and its neighborhood were classified. A training set of ~10-20 images of each kind were created for training. An extended training set of ~ five hundred pictures per species was generated by rotating each picture by twenty-four equidistant angles, as well as rescaling to 90, 100, and 110% of the original size. Training was performed by (on average) two thousand forward passes per extended training set picture, with full error back propagations. Feed-forward and error-backward propagations employ well-known sigmoidal characteristics based on the logistic function. The target signals for the two output neurons were [1, 0] corresponding to E, and [0, 1] corresponding to S, respectively.

2.8. In vitro capillary-like tube formation assay

A 15-well Ibidi angiogenesis microslide (Ibidi, Clinisciences, Nanterren France) was coated with 10 µL of Matrigel matrix (Corning) and incubated for 30 minutes at 37°C for gel polymerization. Twenty thousand HUVECs were seeded on top of the polymerized gel matrix in complete medium with increasing concentrations of PP-13 or 0.1% DMSO. The microslide was then placed in a 37°C heated stage in a 5% CO_2 humidified atmosphere. Images were acquired after 6 h of incubation by a phase-contrast microscope with an Achromat 5×/0.12 NA objective, blinded and analyzed using the automated WimTube image analysis tool (Wimasis GmbH, Munich, Germany).

2.9. In vivo studies using chick embryo tumor model

A chick embryo tumor growth and metastasis assay (InOvotion, Grenoble, France) was performed as previously described [9]. According to French legislation, no ethical approval is needed for scientific experimentations using oviparous embryos (decree number 2013–118, February 1, 2013; art. R-214–88). Briefly, fertilized white leghorn eggs (SFPA, Hendrix Genetics group, Saint Brieuc, France) were incubated at 38°C with 60% relative humidity for nine days. The chorioallantoic membrane (CAM) was then dropped, and a 1-cm^2 window was cut into the eggshell above the CAM (at day nine). A total of three million A549 cells were added directly onto the CAM of each egg. The eggs were randomly allocated into three groups. Group size was determined based on the expertise of InOvotion showing that $n \geq 15$ was the minimum number of eggs to show significant effects. At day ten, when tumors began to be detectable, the eggs were treated every other day for ten days by adding 100 µL of either 50 $\mu mol.L^{-1}$ paclitaxel (n = 17), 0.13 $\mu mol.L^{-1}$ PP-13 (n = 18), or 0.5% DMSO in PBS (vehicle, n = 18) dropwise onto the tumor. The concentration of paclitaxel was chosen as a positive control to induce significant tumor growth inhibition without toxicity for embryos.

The concentration of PP-13 has been arbitrarily chosen according to *in vitro* experiments (IC_{50}) and following the expertise of InOvotion. The upper portion of the CAM was then removed, and the tumors were carefully cut away and weighed. In parallel, a 1-cm^2 portion of the lower CAM was collected, genomic DNA was extracted, and qPCR analysis was performed by using primers specific for genomic human Alu/repetitive sequences [9] to evaluate the number of A549 cells. Finally, scoring the number of dead embryos and looking for morphological or functional abnormalities in the surviving embryos was carried out to evaluate the toxicity of the treatment.

2.10. In vivo studies using mice tumor model

All animal studies were performed in accordance with the European Economic Community guidelines and the "Principles of Laboratory Animal Care" (NIH publication N 86-23 revised 1985) and were approved by the institutional guidelines and the European Community (EU Directive 2010/63/EU) for the use of experimental animals (authorization for the experiment: APAFIS#8854-2017031314338357 v1).

Six-week-old female NMRI nude mice (Janvier Labs, Le Genest-Saint Isle, France) were anesthetized using 4% isoflurane/air for anesthesia induction and 1.5% thereafter, and luciferase-modified mouse 4T1 cancer cells (4T1-rvLuc2 cells, 20000 cells per 50 µL) were injected into the mammary fat pad. The mice were immediately randomly divided into four groups of eight mice, receiving vehicle (0.9% NaCl, 1% DMSO, 30% PEG, 1% Tween-80, referred to as control), 0.5 $mg.kg^{-1}$ paclitaxel, 0.5 $mg.kg^{-1}$ PP-13, or 1 $mg.kg^{-1}$ PP-13. Group size was determined based on our expertise showing that $n \geq 8$ per group was the minimum number of mice to show significant effects on metastases. Based on the results obtained on

chick embryo tumor model showing the effect of PP-13 at very low dose, two low concentrations of PP-13 were chosen (0.5 and 1 $mg.kg^{-1}$). Similar low concentration (0.5 $mg.kg^{-1}$) was chosen for paclitaxel to compared this standard chemotherapy with PP-13, and based on preliminary experiments showing sub-therapeutic effect of 0.5 mg/kg^{-1} paclitaxel on tumor and metastases growth (data not shown). Intraperitoneal administration of 200 µL of treatment was performed three times per week for five weeks. The mice were examined daily for behavior and morbi-mortality and were weighed three times per week. The primary tumor growth was monitored three times per week using a caliper, and the tumor volume was calculated as follows [13]: tumor volume = length x width x 0.4. The thoracic metastasis growth was followed once per week by *in vivo* bioluminescence imaging (IVIS KINETIC, Perkin Elmer, Waltham, MA, USA) 5 min after the intraperitoneal injection of 150 $mg.kg^{-1}$ of luciferin (Promega, E1605), as previously described [14]. Twenty-two days after 4T1-rvLuc2 cell implantation, 0.1 $mg.kg^{-1}$ buprenorphine was injected subcutaneously for analgesia and the primary breast tumors were excised under general anesthesia. The mice were carefully observed during the day following the surgery. After five weeks, the mice were sacrificed and blood samples were collected by cardiac puncture using a heparinized syringe. The lungs, axillary and brachial lymph nodes, kidney and liver were harvested for further imaging and/or analyses.

2.11. Ex vivo studies of mice tissue samples

Blood samples were evaluated for hematological parameters with a medical automated hematology analyzer (Micros-60, Horiba ABX, Montpellier, France), and biochemical analyses were performed by the Charles Rivers Laboratory (Massachusetts, USA). Bone marrow was obtained after having carefully sectioned mice femurs at each joint and flushing

the bone cavity with PBS. Cells from the plasma and bone marrow samples were washed in PBS, cytospun (Cytospin 4, Fisher Scientific, Illkirch, France) and stained with May-Grunwald-Giemsa solution (MGG) with the automated XE-5000 Instrument (Sysmex, Roissy, France). Global cell abundance evaluation and megakaryocyte and leukocyte counting were then performed for both samples by an experienced hematologist.

Tumor tissues were frozen in OCT-embedding medium (VWR international, Fontenay-sous-Bois, France) and cut into 7 µm thick sections using a cryomicrotome for immunohistochemical analyses. Immunohistochemical examinations were performed after fixation with 4% paraformaldehyde and staining with anti-CD31 antibody (Pharmingen, BD Biosciences, Le Pont de Claix, France), using an AxioImager M2 microscope (Carl Zeiss, Jena, Germany). Segmentation of tissues was performed using a fully connected, three-layer back-propagation neuronal network, as previously described [12].

2.12. Statistical analyses

All analyses were performed using the GraphPad Prism software (GraphPad Software Inc., San Diego, California, USA). Statistical comparisons between two groups or more were conducted with Mann-Whitney test, Kruskal-Wallis test, or Friedman test with Dunn's multiple comparisons post hoc test. Statistical comparisons between mice groups among time were determined by two-way ANOVA with Bonferroni's post hoc test. Statistical significance was defined for p values ≤ 0.05.

3. Results

3.1. PP-13 treatment decreases cancer cell proliferation in vitro

To investigate the therapeutic effect of PP-13, we chose three cell lines displaying high levels of proliferation, migration and invasiveness: the human HeLa cervical cell line and its derivative subclone expressing mEGFP-α-tubulin and mRFP-H2B (HeLa-EGFP/RFP), the human A549 lung cancer cell line, and the mouse 4T1 mammary cancer cells expressing mRFP-H2B (4T1-RFP) or luciferase (4T1-rvLuc2). We first analyzed the toxicity of PP-13 in these cell lines cultured in monolayers or in 3D-spheroids. PP-13 had a significant effect on the proliferation of these cell lines, strongly reducing their viability (Fig. 1A). The IC_{50} values of PP-13 (50% growth inhibition) were relatively similar for the three cell lines cultured in monolayers (Table 1) [9]. These IC_{50} values did not vary significantly when the cells were grown in spheroids, except for A549 (Table 1 and Fig. 1A and 1B). Indeed, the A549 spheroids appeared to strongly resist PP-13 treatment compared to A549 cells in the monolayer cell culture. Similar effects were observed in these cell lines with the reference antimitotic chemotherapy paclitaxel (Table 1 and Fig. 1). We have shown that paclitaxel has a reducing effect on 4T1 cell viability in 2D culture compared to A549 (~five-fold lower) and HeLa (~ten-fold lower) cells, thus reflecting the resistance of 4T1 cells to paclitaxel. In addition, although 4T1-RFP spheroids were surprisingly more sensitive to low doses of paclitaxel than monolayer 4T1-RFP cells, high concentrations of paclitaxel failed to inhibit more than 50% of the cell proliferation of both A549 and 4T1 spheroids. Thus, PP-13 affected the proliferation of invasive cells *in vitro*, including those that are resistant to paclitaxel.

3.2. PP-13 treatment induces mitotic blockade in cancer cell spheroids

We previously demonstrated that PP-13 induced a transient mitotic blockade by interfering with mitotic spindle organization and microtubule dynamics in monolayer cell cultures [9].

Here, we analyzed the effect of PP-13 on mitosis in spheroids. The cell viability of HeLa-EGFP/RFP spheroids was not impacted by a short 24 h treatment of 200 nmol.L^{-1} PP-13 (data not shown). Alpha-tubulin and phosphorylated histone H3 (H3P), a marker of late G_2/M cell cycle phase, were analyzed by confocal microscopy on HeLa-EGFP/RFP spheroid sections (Fig. 2A). We observed that PP-13 led to mitotic defects, including multiple misoriented and shortened mitotic spindles (green arrows) associated with chromosomes miscongression (blue arrows). In addition, we showed a significant increase in the level of H3P after 24 h of PP-13 treatment, reflecting the strong accumulation of cells in mitosis in the HeLa-EGFP/RFP spheroids (Fig. 2C). As expected, paclitaxel also enhanced the level of H3P in HeLa-EGFP/RFP spheroids but to a lower extent than PP-13 and with an effect mainly on the cells at the periphery of the spheroids (Fig. 2B and 2C). Accumulation of H3P in response to PP-13 treatment was also increased in A549 spheroids compared to untreated control (Fig. 2C), and was confirmed by western blot of the three spheroid types (Fig. 2D). Finally, after 72 h of PP-13 treatment, the HeLa-EGFP/RFP spheroids showed a significant increase in cleaved caspase-3 (Fig. 2E and 2F). Therefore, in spheroid cultures, PP-13 induced mitotic spindle disorganization, mitotic blockade, inhibition of cell growth and apoptosis.

3.3. PP-13 inhibits angiogenesis in vitro

Because most of the microtubule-targeting agents also exhibit antiangiogenic properties [3, 6, 15, 16], we investigated the effects of PP-13 on capillary-like structure formation *in vitro* using HUVECs plated on a Matrigel basement membrane. In control conditions, endothelial cells aligned and formed organized networks of capillary-like structures after 6 h (Fig. 3A). PP-13 treatment reduced the total number of branching points, the number of loops, the length of the tubes, and the total cell-covered area compared to the control (Fig. 3B). Altogether, PP-

13 altered the ability of HUVECs to form tube-like structures. The concentrations of PP-13 that were used had limited impact on HUVEC proliferation (Fig. 3C). Hence, this suggested that PP-13 displayed antiangiogenic properties in vitro.

3.4. PP-13 inhibits the migration of cancer cells in vitro

Given the essential role of microtubules in cell motility, we investigated whether the PP-13 tubulin inhibitor impacted HeLa, A549, and 4T1-rvLuc2 cell migration and invasiveness in vitro. The impact of PP-13 on the motility of cells was examined using an in vitro wound-healing assay. We observed that PP-13 significantly reduced the motility of the three cell lines in a dose-dependent manner, and as paclitaxel (Fig. 4A and 4B). The effect of PP-13 on invasive migration was assessed with Matrigel in transwell chambers. PP-13 exerted a strong inhibitory effect on the invasion of the three cell lines (Fig. 4C and 4D). Paclitaxel also inhibited the invasion of these cells. These results indicated that PP-13 is able to slow down cell motility and invasion in vitro.

3.5. PP-13 inhibits the migration of cancer cells in vivo

We previously showed that PP-13 reduces tumor growth and metastatic invasion *in vivo* by using H358 NSCLC cells engrafted onto chicken chorioallantoic membranes (CAMs) [9]. Here, we used A549 NSCLC cells engrafted onto the CAMs to evaluate the efficacy of PP-13 on the migration of invasive cancer cells. The tumors were treated every other day with vehicle (control), PP-13, or paclitaxel (Fig. 5A). At the end of the experiment, the tumors were recovered from the upper CAMs and weighed. We used a very low concentration of PP-13 (0.13 µmol.L-1) compared to the > 10 µmol.L-1 PP-13 IC_{50} in the A549 spheroid cell

culture (Table 1), which did not inhibit A549 tumor growth (Fig. 5B). Analysis of the presence of A549 cells at the lower CAM by qPCR, allowing for the accurate detection of tumor cell dissemination, showed that this low dose of PP-13 significantly reduced the metastatic ability of A549 cells compared to the control (Fig. 5C). Paclitaxel was used as a positive control at a concentration known to inhibit A549 tumor growth and metastatic dissemination without inducing significant toxicity (Fig. 5B and 5C) [9]. These results suggested that PP-13 inhibited invasion in vivo. Furthermore, treatment with PP-13 did not significantly increase the mortality (two embryos died in the control group, and one embryo died in both paclitaxel and PP-13-treated groups) or abnormalities (no abnormality observed on surviving embryos for the different experimental groups) on chicken embryos, indicating that it was well tolerated.

3.6. PP-13 impairs tumor progression and metastasis in an allogeneic breast cancer model

To further evaluate the effect of PP-13 on tumor growth and metastasis formation, we used the allogeneic model of 4T1-rvLuc2 cell engraftment in the mammary fat pads of mice. We chose this model because once engrafted orthotopically in the mammary gland, 4T1-rvLuc2 mouse cancer cells metastasize to multiple distant sites (lymph nodes, lungs, liver, bone, brain), thus mimicking human breast cancers [17]. As soon as the 4T1-rvLuc2 cells were inoculated, the mice were randomly divided into four groups: one control group, one group treated with paclitaxel (0.5 $mg.kg^{-1}$) and two groups treated with PP-13 (0.5 and 1 $mg.kg^{-1}$) (Fig. 5D). The low concentrations of PP-13 were chosen based on the results obtained on chick embryo tumor model showing an inhibitory effect of PP-13 at very low dose, and were compared to the same concentration of the standard chemotherapy paclitaxel. Intraperitoneal

injections of each treatment were performed three times per week. The tumor progression was not affected at early time points, but the final tumor volumes were significantly lower after three weeks for the two groups treated with PP-13 in this rapidly progressing breast cancer model (Fig. 5E). The potential antiangiogenic activity of PP-13 in vivo was assessed sections performed on primary tumors stained with an anti-CD31 antibody. The microvessel density was counted and showed no significant difference between the treatments at the concentrations used and at this time-point (Fig. 5F). No significant difference between the treatments was observed in Ki67 immunostaining either (data not shown).

In vivo bioluminescence imaging was used to follow the development of thoracic metastases before and after primary tumor resection. Paclitaxel had no effect on the bioluminescence signal compared to the control treatment and even slightly enhanced it at day 28 (Fig. 6A and 6B). In contrast, the signal of thoracic metastasis was reduced with PP-13 treatment. Of note, both PP-13 and paclitaxel treatment reduced the number of mice with thoracic metastases compared to the control treatment from 2 weeks of treatment (Table 2). These results were confirmed by measuring bioluminescence in the lungs ex vivo at the end of the experiment (day 35) (Fig. 6C). This showed a non-significant 66% reduction in the lung metastasis signal in mice treated with 1 $mg.kg^{-1}$ PP-13 compared to control mice (Fig. 6D). In addition, ex vivo, the axillary and brachial lymph nodes showed a significant decrease in signal in both of the PP-13-treated groups compared to the control and paclitaxel-treated groups (Fig. 7A and 7B). The percentage of mice with axillary and brachial lymph node metastases was reduced in a dose-dependent manner in the PP-13-treated groups compared to the control and paclitaxel-treated groups (Table 2), as was the number of metastatic axillary and brachial lymph nodes (Fig. 7A). Taken together, these results showed that PP-13 decreased tumor and metastatic dissemination in this breast cancer model.

3.7. PP-13 shows no adverse side effects in vivo

We assessed the toxicity of PP-13 and paclitaxel *in vivo*. There was no body-weight loss in the control and PP-13-treated mice over the course of the experiment, while mice exposed to paclitaxel displayed a significant decrease in body weight at the end of the experiment (Table 3). In addition, one of the eight mice in each of the paclitaxel and control groups died before the end of the experiment probably because of tumor progression, while all PP-13-treated mice survived suggesting that PP-13 may control tumor progression.

We paid particular attention to some of the side effects described for conventional spindle poisons in patients. Serum biochemical analysis showed significant decreases in phosphorus, creatinine, and glucose in paclitaxel-treated mice compared to the control group (Table 4). No significant changes in serum biochemical values were reported in PP-13-treated mice, except a small and isolated decrease in blood urea nitrogen that did not reflect any renal toxicity in this context. In addition, macroscopic analyses of the organs of the treated mice did not show evidence of damage (data not shown). Hematological analysis of the blood and bone marrow cells from mice treated with PP-13 did not reveal any apparent signs of myelosuppression or other hematological abnormalities compared to the control (Table 5). In contrast, paclitaxel treatment led to a significant reduction in the white blood cell (WBC) count and a slight increase in the mean corpuscular hemoglobin concentration (MCHC).

Overall, these data suggest that PP-13 displays a favorable safety profile, as it slows both tumor and metastasis progression and is well tolerated at these doses compared to the control and paclitaxel.

4. Discussion

The new pyrrolo[2,3d]pyrimidine-based colchicine-binding site agent PP-13 showed promising anticancer properties *in vitro* [9]. In this study, we explored the therapeutic potential of PP-13, particularly in conditions leading to invasive cancer cell phenotype, and compared the effects of PP-13 with those of paclitaxel, a widely used tubulin-targeting agent in solid tumors. We showed that PP-13 inhibited proliferation, migration and angiogenesis in vitro, which may potentiate its antineoplastic activity, and reduced metastatic dissemination in paclitaxel-resistant tumors in vivo, with no detectable adverse side effects.

We confirmed the in vitro antitumor effects of PP-13 in spheroids. The PP-13-treated spheroids showed enhanced H3P levels associated with defects in mitotic spindle organization and chromosome congression, thus confirming in three-dimensions models that PP-13 induced an early mitotic blockade. Late caspase-3-dependent apoptotic mechanisms contributed to the decrease in spheroid growth, as was previously described in two-dimensions cell cultures [9]. Spheroids are currently considered to be a more suitable model than monolayer cell cultures because they better mimic the *in vivo* three-dimensions tumor environment and cell-cell and cell-extracellular matrix interactions [18-20]. Large spheroids ($\geq$ 300 μm diameter), such as those generated in our experiments, display a hypoxic core resulting from chemical gradients of oxygen and nutrients that are correlated with chemoresistance, as reported in developing tumors [21]. We observed differences in the IC_{50} values of PP-13 between monolayer cell culture and spheroids. In particular, A549 cells were resistant to PP-13 when cultured in spheroids, in contrast to monolayer cell culture, suggesting that the effect of PP-13 observed on two-dimensions-culture cell proliferation is reduced in spheroids. The presence of various environmental factors affecting the tumor development (e.g., cell–cell adhesion, cell-cycle distribution, local pH, extracellular matrix)

[20] could explain the lower sensitivity of spheroid cancer cells to drugs compared to two-dimensions cell cultures, as was also observed in different in vivo tumor models [22-24]. The physicochemical properties of PP-13 could also be responsible for the lower sensitivity in three-dimensions cell culture.

Despite opposite mechanisms of action (microtubule stabilization or depolymerization) [3], both PP-13 and paclitaxel lead to the disruption of the microtubule organization and the induction of cancer cell cycle arrest and apoptosis.

Angiogenesis and cancer cell migration are attractive therapeutic targets [25]. The widely used capillary-like tube formation assay aids in studying the effects of new molecules on many steps of neoangiogenesis, including endothelial cell adhesion, migration, and tubule formation [26]. With this approach, we showed that PP-13 interfered with the tubule assembly in vitro by decreasing both the number of loops and branch nodes, the total length of the formed tubes and the cell-covered area. Using in vivo 4T1 primary breast tumor models, we did not observe any impact of PP-13 on microvessel density, suggesting that such PP-13 concentrations were inadequate to induce antiangiogenic activities and/or that the study time was not suitable to inhibit endothelial cells in vivo in this rapidly progressing breast cancer orthotopic model.

PP-13 inhibited cell motility and invasion both in vitro and in vivo. In vitro, we found that PP-13 inhibited cancer cell migration in the three metastatic tumor cell types. In addition, PP-13 reduced metastatic invasion in H358 [9] and A549 NSCLC cells engrafted onto chicken CAMs at concentrations that did not inhibit cell proliferation in A549 spheroids. Accordingly, PP-13 did not inhibit A549 tumor growth in chicken CAMs. This confirmed the lower effect of PP-13 on cell proliferation in spheroids and in vivo compared to monolayer cell culture.

The orthotopic mouse model of breast cancer that was used is clinically relevant to predict the influence of the organ microenvironment on tumor cell behavior and to study the cancer cell invasion and metastatic growth [27]. Although PP-13 did not inhibit in vivo tumor cell migration and metastasis seeding at the concentrations used, we observed that the growth of the metastases was delayed, and their size remained small in both lungs and lymph nodes when the cells migrated from the primary tumor. Although PP-13 had both antiproliferative and antimigration effects in vitro, the in vivo experiments indicated that the effect of the drug on the inhibition of invasion was stronger than its antiproliferative effects.

Overall, our data indicate that PP-13 could be a potent agent to decrease the growth of both primary tumors and their metastases, especially for triple-negative breast cancers (TNBC), which account for nearly 15% of breast cancers and have poor therapeutic options and prognoses [28]. The 4T1 allogeneic transplant mouse model mimics TNBC in humans and is associated with a high propensity to metastasize, primarily in the lymph nodes and lungs. The therapeutic arsenal for TNBC mainly consists of anthracyclines and taxane-based chemotherapies; however, the emergence of resistance and frequent tumor recurrence support the need to identify alternative drugs for the management of refractory tumors. The 4T1 model thus represents an interesting approach to screen new molecules for TNBC therapy, especially since it spontaneously metastasizes in the same regions as in TNBC and easily develops resistance to chemotherapies classically used in TNBC [29, 30]. Compared to paclitaxel, which was used as a reference treatment to reduce metastasis while limiting the adverse effects, PP-13 moderately inhibited primary tumor growth and delayed metastatic growth.

PP-13 treatment did not show any sign of toxicity compared to the controls; there was notably an absence of myelosuppression, which is classically observed with conventional antimitotic drug treatments or colchicine binding-site agents [3]. At the same dose, paclitaxel led to a significant decrease in white blood cell count, as has been previously reported [31], as well as a slight reduction in plasma glycaemia, phosphorus and creatinine and an increase in MCHC. Further investigations with higher concentrations of PP-13 will be needed to establish the maximal antitumor effect of PP-13, ~~and~~ the therapeutic index of the molecule, and long-term survival. In addition, PP-13 has no kinase activity [9] but may target other molecule than tubulin, that remains to determine.

In summary, PP-13 significantly reduced the cancer cell migration and neoangiogenesis processes in vitro. PP-13 also led to a reduction in both tumor growth and metastatic dissemination in vivo in a mouse orthotopic TNBC model without any significant toxicity. These findings suggest that PP-13 should be an efficient anticancer therapy and an *alternative* option to conventional spindle poisons such as taxanes or vinca-alkaloids.

5. Acknowledgements

We acknowledge the assistance of Alexeï Grichine, Mylène Pezet and Jacques Mazzega (Optical Microscopy Platform - Cell Imaging, INSERM U1209). We kindly thank Dr. Lucie Sancey for critical evaluation of the data, and Lilya Mediouni for her help. This work was supported by the Institut Curie, the CNRS, the INSERM, and grants from “La Fondation de France” and “La Ligue contre le Cancer (comité de l’Isère)”. The *in vivo* evaluation was performed by the OPTIMAL facility, which is part of the France Live Imaging Program (FLI-

Grenoble; French program “Investissement d’Avenir”; grant “Infrastructure d’avenir en Biologie Santé,” ANR-11-INBS-0006).

6. Author contributions

PG, BB, and AH conceived the project, designed the experiments, and interpreted the data. PG, LL, MC, LV, MH, and JV were involved in acquisition, analysis and interpretation of the data. VB, MW, and AO managed automated quantifications. VJ, MH, and JV designed the *in vivo* experiment. FMB synthesized and characterized PP-13. JLC, BB and AH supervised the research and analyses. PG, BB and AH supervised the whole project and wrote the manuscript. All authors reviewed the manuscript.

7. References

[1] K.D. Miller, R.L. Siegel, C.C. Lin, A.B. Mariotto, J.L. Kramer, J.H. Rowland, et al., Cancer treatment and survivorship statistics, 2016, CA Cancer J Clin 66(4) 2016: 271-89.

[2] M.A. Jordan, L. Wilson, Microtubules as a target for anticancer drugs, Nat Rev Cancer 4(4) 2004: 253-65.

[3] C. Dumontet, M.A. Jordan, Microtubule-binding agents: a dynamic field of cancer therapeutics, Nat Rev Drug Discov 9(10) 2010: 790-803.

[4] M.A. Jordan, Mechanism of action of antitumor drugs that interact with microtubules and tubulin, Curr Med Chem Anticancer Agents 2(1) 2002: 1-17.

[5] D. Fanale, G. Bronte, F. Passiglia, V. Calo, M. Castiglia, F. Di Piazza, et al., Stabilizing versus destabilizing the microtubules: a double-edge sword for an effective cancer treatment option?, Anal Cell Pathol (Amst) 2015 2015: 690916.

[6] E.L. Schwartz, Antivascular actions of microtubule-binding drugs, Clin Cancer Res 15(8) 2009: 2594-601.

[7] C. Kanthou, G.M. Tozer, Microtubule depolymerizing vascular disrupting agents: novel therapeutic agents for oncology and other pathologies, Int J Exp Pathol 90(3) 2009: 284-94.

[8] D. Bates, A. Eastman, Microtubule destabilising agents: far more than just antimitotic anticancer drugs, Br J Clin Pharmacol 83(2) 2017: 255-268.

[9] P. Gilson, J.F. Josa-Prado, C. Beauvineau, D. Naud-Martin, L. Vanwontherghem, F. Mahuteau-Betzer, et al., Identification of pyrrolopyrimidin derivative PP-13 as a novel microtubule-destabilizing agent with promising anticancer properties, Scientific Reports 7 2017: 10209.

[10] P. Steigemann, C. Wurzenberger, M.H. Schmitz, M. Held, J. Guizetti, S. Maar, et al., Aurora B-mediated abscission checkpoint protects against tetraploidization, Cell 136(3) 2009: 473-84.

[11] B. Busser, L. Sancey, V. Josserand, C. Niang, M.C. Favrot, J.L. Coll, et al., Amphiregulin promotes BAX inhibition and resistance to gefitinib in non-small-cell lung cancers, Molecular therapy 18(3) 2010: 528-35.

[12] Q. Zheng, B.K. Milthorpe, A.S. Jones, Direct neural network application for automated cell recognition, Cytometry A 57(1) 2004: 1-9.

[13] B. Busser, L. Sancey, V. Josserand, C. Niang, S. Khochbin, M.C. Favrot, et al., Amphiregulin promotes resistance to gefitinib in nonsmall cell lung cancer cells by regulating Ku70 acetylation, Molecular therapy 18(3) 2010: 536-43.

[14] V. Jeannot, S. Mazzaferro, J. Lavaud, L. Vanwonterghem, M. Henry, M. Arboleas, et al., Targeting CD44 receptor-positive lung tumors using polysaccharide-based nanocarriers: Influence of nanoparticle size and administration route, Nanomedicine 12(4) 2016: 921-32.

[15] E. Pasquier, S. Honore, D. Braguer, Microtubule-targeting agents in angiogenesis: where do we stand?, Drug Resist Updat 9(1-2) 2006: 74-86.

[16] E. Pasquier, N. Andre, D. Braguer, Targeting microtubules to inhibit angiogenesis and disrupt tumour vasculature: implications for cancer treatment, Curr Cancer Drug Targets 7(6) 2007: 566-81.

[17] B.A. Pulaski, S. Ostrand-Rosenberg, Mouse 4T1 breast tumor model, Curr Protoc Immunol Chapter 20 2001: Unit 20 2.

[18] C.J. Lovitt, T.B. Shelper, V.M. Avery, Advanced cell culture techniques for cancer drug discovery, Biology (Basel) 3(2) 2014: 345-67.

[19] F. Hirschhaeuser, H. Menne, C. Dittfeld, J. West, W. Mueller-Klieser, L.A. Kunz-Schughart, Multicellular tumor spheroids: an underestimated tool is catching up again, Journal of biotechnology 148(1) 2010: 3-15.

[20] G. Mehta, A.Y. Hsiao, M. Ingram, G.D. Luker, S. Takayama, Opportunities and challenges for use of tumor spheroids as models to test drug delivery and efficacy, Journal of controlled release : official journal of the Controlled Release Society 164(2) 2012: 192-204.

[21] S. Daster, N. Amatruda, D. Calabrese, R. Ivanek, E. Turrini, R.A. Droeser, et al., Induction of hypoxia and necrosis in multicellular tumor spheroids is associated with resistance to chemotherapy treatment, Oncotarget 8(1) 2017: 1725-1736.

[22] R. Edmondson, J.J. Broglie, A.F. Adcock, L. Yang, Three-dimensional cell culture systems and their applications in drug discovery and cell-based biosensors, Assay Drug Dev Technol 12(4) 2014: 207-18.

[23] S. Breslin, L. O'Driscoll, The relevance of using 3D cell cultures, in addition to 2D monolayer cultures, when evaluating breast cancer drug sensitivity and resistance, Oncotarget 7(29) 2016: 45745-45756.

[24] V.S. Nirmalanandhan, A. Duren, P. Hendricks, G. Vielhauer, G.S. Sittampalam, Activity of anticancer agents in a three-dimensional cell culture model, Assay Drug Dev Technol 8(5) 2010: 581-90.

[25] D. Hanahan, R.A. Weinberg, Hallmarks of cancer: the next generation, Cell 144(5) 2011: 646-74.

[26] D. Xie, D. Ju, C. Speyer, D. Gorski, M.A. Kosir, Strategic Endothelial Cell Tube Formation Assay: Comparing Extracellular Matrix and Growth Factor Reduced Extracellular Matrix, J Vis Exp (114) 2016.

[27] S. Man, R. Munoz, R.S. Kerbel, On the development of models in mice of advanced visceral metastatic disease for anti-cancer drug testing, Cancer Metastasis Rev 26(3-4) 2007: 737-47.

[28] P. Kaur, G.M. Nagaraja, H. Zheng, D. Gizachew, M. Galukande, S. Krishnan, et al., A mouse model for triple-negative breast cancer tumor-initiating cells (TNBC-TICs) exhibits similar aggressive phenotype to the human disease, BMC Cancer 12 2012: 120.

[29] L. Bao, A. Haque, K. Jackson, S. Hazari, K. Moroz, R. Jetly, et al., Increased expression of P-glycoprotein is associated with doxorubicin chemoresistance in the metastatic 4T1 breast cancer model, Am J Pathol 178(2) 2011: 838-52.

[30] T. Luo, J. Wang, Y. Yin, H. Hua, J. Jing, X. Sun, et al., (-)-Epigallocatechin gallate sensitizes breast cancer cells to paclitaxel in a murine model of breast carcinoma, Breast Cancer Res 12(1) 2010: R8.

[31] E.A. Perez, Paclitaxel in Breast Cancer, Oncologist 3(6) 1998: 373-389.

Figure legends

Table 1: Sensitivity of cancer cell lines to PP-13 and paclitaxel. The drug concentrations required to inhibit cell growth by 50% (IC_{50}) at 72h in HeLa cells, HeLa mEGFP-α-tubulin and mRFP-H2B cells (HeLa-EGFP/RFP), A549 cells, 4T1 mRFP-H2B cells (4T1-RFP) and 4T1-rvLuc2 cells cultured in 2D-monolayer (2D) or spheroids. Data represent the mean ± SD of three independent experiments, each performed in triplicate.

Table 2: PP-13 decreased the number of mice with thoracic and lymph node metastases. Mice with 4T1-rvLuc2 tumors were treated with vehicle (control), paclitaxel 0.5 $mg.kg^{-1}$, or PP-13 (0.5 and 1 $mg.kg^{-1}$) (see Fig. 5D). Number and percentages of mice with thoracic metastases at day 14, and with invaded axillary and brachial lymph nodes at day 35 are shown in each group.

Table 3: Mice body-weight. Mice with 4T1-rvLuc2 tumors were treated with vehicle (control), paclitaxel 0.5 $mg.kg^{-1}$, or PP-13 (0.5 and 1 $mg.kg^{-1}$) (see Fig. 5D). Mice body-weight is expressed as mean ± SEM (n=8, except in paclitaxel-treated group at day 35, n=7), and as percentage of initial body-weight (day 0). * p <0.05; two-way ANOVA with Bonferroni post-test (day 35 compared to day 28).

Table 4: Biochemical analyses of mice. Plasma biochemical values of mice after control, paclitaxel or PP-13 treatments were assessed. Data represent the mean ± SD of 6 mice per group. Data were analyzed using Mann-Whitney *U*-test. * Significant as compared to control group.

Table 5: Hematological and bone marrows analyses of mice. Complete blood count and white blood cells count and evaluation of the global cell abundance and megakaryocyte and leukocyte counts in the bone marrow, from mice treated with control, paclitaxel, or PP-13. Data represent the mean ± SD of 8 mice per group. # from score 1 (low abundance) to score 4 (high abundance). Data were analyzed using one-way analysis of variance. NS: not significant.

Figure 1: Viability of cancer cells treated with PP-13 or paclitaxel.

A. A549, 4T1 mRFP-H2B (4T1-RFP), and HeLa mEGFP-α-tubulin mRFP-H2B (HeLa-EGFP/RFP) were cultured in two-dimensions (2D) or in spheroids, and treated for 72 h with increasing concentrations of PP-13 (left) or paclitaxel (right), and the cell viability was assessed. Data represent the mean ± SD from three independent experiments, each performed in triplicate. **B.** Representative images of treated spheroids are shown. Bars: 100 µm.

Figure 2: Effects of PP-13 on cancer cell spheroids.

HeLa mEGFP-α-tubulin mRFP-H2B (HeLa-EGFP/RFP) spheroids were treated with vehicle (control), 200 nmol.L^{-1} PP-13, or 15 nmol.L^{-1} paclitaxel for 24 h (**A-D)** or for 72 h (**E-F**). A549 spheroids were treated for 24 h with vehicle (control) or 10 µmol.L^{-1} PP-13 (**C-D**). 4T1 mRFP-H2B (4T1-RFP) spheroids were treated for 24 h with vehicle (control) or 200 nmol.L^{-1} PP-13 (**D**). **A.** Representative confocal microscopy images of microtubules (α-tubulin-EGFP) and phosphorylated histone H3 (H3P, a marker of late G_2/M cell cycle phase) immunodetection in spheroid sections treated with vehicle (control) or PP-13. In purple: H3P, in green: α-tubulin, in red: H2B-RFP, in blue: Hoechst-stained nuclei. The green and blue arrows indicate multipolar mitotic spindles and miscongressed chromosomes, respectively. Scale bars: 50 µm (20x magnification) and 10 µm (63x magnification). **B.** Representative

confocal microscopy images of H3P analyzed by immunofluorescence on spheroids sections treated with vehicle (control), or paclitaxel. In pink: H3P, in blue: Hoechst-stained nuclei. Scale bars: 50 µm. **C.** The percentage of H3P was calculated as the number of H3P-positive cells in control (n = 7, HeLa-EGFP/RFP; n=11, A549), PP-13 (n = 13, HeLa-EGFP/RFP; n=11, A549), or paclitaxel (n = 9, HeLa-EGFP/RFP) spheroids, with two or three sections per spheroid. Data are expressed as the mean ± SD. *** $p < 0.0001$ between control and treated conditions; Mann-Whitney *U*-test. **D.** Western blot analysis of H3P in A549, 4T1-RFP, or HeLa-EGFP/RFP pooled spheroids (n = 10 spheroids in each condition). Actin was used as a loading control. Values indicate relative H3P/actin ratio. **E.** Representative confocal microscopy images of cleaved caspase-3 immunodetection in spheroid sections. In purple: cleaved caspase-3, in green: α-tubulin, in red: H2B-RFP, in blue: Hoechst-stained nuclei. Scale bars: 50 µm. **F.** Quantification of cleaved caspase-3 in spheroids (control, n = 9 spheroids; PP-13, n = 7 spheroids; with two or three sections per spheroids). Data are expressed as the mean ± SD. *** $p < 0.0001$ between control and treated conditions; Mann-Whitney *U*-test.

Figure 3: In vitro effects of PP-13 on angiogenesis.

HUVECs were treated with vehicle (control) or increasing concentrations of PP-13, as indicated, for 6 h. **A.** Capillary-like tube formation assay: representative images of the HUVEC capillary-like tube formation in each condition. Bar: 200 µm. **B.** Quantification of the tube length, the cell-covered area, the number of loops and the number of branching points. Data are expressed as the mean ± SD and as the percentages of vehicle condition to control the seeding variations between the experiments (n = 5). * $p < 0.05$; ** $p < 0.01$; *** $p < 0.001$ between control and treated conditions; Kruskal-Wallis test with Dunn's multiple

comparisons post hoc test. **C.** HUVEC cell viability was assessed. Data represent the mean ± SD ($n \geq 3$).

Figure 4: In vitro effects of PP-13 on cancer cell migration and invasion.

A-B. Wound-healing assay in A549, HeLa, and 4T1-rvLuc2 cells treated with vehicle (control) or increasing concentrations of PP-13 or paclitaxel for 12 h. **A.** Representative images from wound-healing assay experiment at 0 h and 12 h. Cells were treated with vehicle (control), 1 $\mu mol.L^{-1}$ (A549 and HeLa) or 0.5 $\mu mol.L^{-1}$ (4T1-rvLuc2) PP-13, 20 $nmol.L^{-1}$ (HeLa) or 50 $nmol.L^{-1}$ (A549) or 200 $nmol.L^{-1}$ (4T1-rvLuc2) paclitaxel. The white lane delineates the edges of the wound. **B.** Relative wound density over time in cells treated as indicated. The relative wound density at 0 h is arbitrarily set to 0%. Data are expressed as the mean ± SD. Experiments were performed at least five times in triplicate. * $p < 0.05$; ** $p < 0.01$; *** $p < 0.001$ compared to control or treated conditions as indicated; Friedman test with Dunn's multiple comparisons post hoc test. **C-D.** Matrigel invasion assay of A549, 4T1-rvLuc2 and HeLa cells treated treated with vehicle (control), 200 $nmol.L^{-1}$ (4T1-rvLuc2) or 500 $nmol.L^{-1}$ (A549, HeLa) PP-13, or 20 $nmol.L^{-1}$ (HeLa), 40 $nmol.L^{-1}$ (A549), or 150 $nmol.L^{-1}$ (4T1-rvLuc2) paclitaxel for 24 h. **C.** Representative images from methylen-blue stained cells treated with vehicle (control), PP-13, or paclitaxel. The red squares show the quantified cells. **D.** Quantification of invasion of cells treated with vehicle (control), PP-13, or paclitaxel. Cells were counted in ten fields per condition and in three independent experiments. Data are expressed as the mean ± SD and as the percentages of vehicle condition to control variations between the experiments. * $p < 0.05$; ** $p < 0.01$ between control and treated conditions; Mann-Whitney *U*-test.

Figure 5: Effects of PP-13 in vivo.

A. Schematic representation of the *in ovo* assay principle. A549 cells were engrafted onto chick embryo chorioallantoic membranes (CAMs) at E9, were randomized into three groups, and treatments with 0.5% DMSO (control, n = 18), 50 $\mu mol.L^{-1}$ paclitaxel (positive control of tumor growth inhibition, n = 17), or 0.13 $\mu mol.L^{-1}$ PP-13 (low dose, n = 18) were administered every other day for 10 days. **B.** Tumors were excised and weighted at the end of the treatments. The histogram represents the effect of treatments on A549 tumor weight (means ± SEM, n = 16). *** $p < 0.001$ compared to control; Kruskal-Wallis test. **C.** The presence of A549 cells in the lower CAM at the end of the experiment was evaluated by qPCR in ten random embryos per group. The histogram represents the effect of treatments on A549 metastases in the lower CAM (means ± SEM, n = 10). The relative amount of metastases in the lower CAM in the control group is arbitrarily set to one to control interindividual variations. *** $p < 0.001$ compared to control; Kruskal-Wallis test.

D. Schematic representation of orthotopic breast tumors and metastatic growth and of the treatment plan. The mice were inoculated with 4T1-rvLuc2 cells and randomized into four groups of eight mice. Vehicle (control), 0.5 $mg.kg^{-1}$ paclitaxel, or 0.5 or 1 $mg.kg^{-1}$ PP-13 were administered intraperitoneally three times a week. Thoracic bioluminescence imaging was performed once a week for five weeks. After three weeks, the primary tumors were resected. **E.** Primary tumor volume. Data represent the mean ± SEM in each group (n = 8). *** $p < 0.001$ compared to control group; two-way ANOVA with Bonferroni post hoc test. **F.** Histogram shows the CD31 positive staining quantification on frozen 4T1-tumor sections, expressed as the mean ± SD. The CD31 levels were determined after counting positive stained blood vessel area as described in methods, in three sections per tumor and in three tumors per group.

Figure 6: Effects of PP-13 on thoracic metastases in orthotopic breast tumor model.

Mice with 4T1-rvLuc2 tumors were treated with vehicle (control), paclitaxel 0.5 $mg.kg^{-1}$, or PP-13 (0.5 and 1 $mg.kg^{-1}$), 3 times a week (see Fig. 5D). **A.** *In vivo* bioluminescence images of the thoracic metastases (ventral view) in one representative mouse per group at day twenty-eight. **B.** Overtime quantification of *in vivo* bioluminescence signal in thoracic areas over the duration of the experiment (ventral and dorsal views). Data are expressed as the mean ± SEM (n = 8). * $p < 0.05$; **** $p < 0.0001$ compared to control or to paclitaxel-treated groups; two-way ANOVA with Bonferroni post hoc test. **C.** Ex vivo bioluminescence images of lungs at the end of the experiment (day 35). (n = 8, except in paclitaxel-treated group, n = 7). **D.** E*x vivo* bioluminescence signal in each lung at the end of the experiment (day 35). Bars: mean bioluminescence signal (n = 8, except in paclitaxel-treated group, n = 7). Number indicates the reduction (%) in mean bioluminescence signal in 1 $mg.kg^{-1}$ PP-13-treated group, compared to control group.

Figure 7: Effects of PP-13 on lymph node metastases.

Axillary and brachial lymph nodes were collected at the end of the experiment (day thirty-five) in 4T1-rvLuc2 mice treated as indicated. **A**. *Ex vivo* bioluminescence images of lymph nodes. RA, right axillary lymph node; LA, left axillary lymph node; RB, right brachial lymph node; LB, left brachial lymph node. Each line shows the lymph nodes of one mouse (n = 8, except in paclitaxel-treated group, n = 7). Numbers indicates the invaded lymph nodes and their percentages in each group. **B.** Ex vivo bioluminescence signal in each lymph node. Bars: median bioluminescence signal (n = 32 lymph nodes/group, 8 mice/group except in paclitaxel-treated group: 7 mice, 28 lymph nodes). * $p < 0.05$; *** $p < 0.001$; **** $p < 0.0001$ compared to control or treated groups; Kruskal-Wallis with Dunn's multiple comparisons post hoc test. ns, not significant.

Table 1: Sensitivity of cancer cell lines to PP-13 and paclitaxel

Cell lines and condition		PP-13 IC_{50} [$nmol.L^{-1}$]	Paclitaxel IC_{50} [$nmol.L^{-1}$]
HeLa	2D	120 ± 10.0	4.0 ± 3.5
HeLa-EGFP/RFP	2D	75 ± 7.1	2.8 ± 0.4
	Spheroids	185 ± 49.5	17 ± 0.6
A549	2D	120 ± 40	9 ± 4.9
	Spheroids	> 10,000	> 500
4T1-RFP	2D	66.5 ± 2.1	35 ± 2.1
	Spheroids	200 ± 5.8	17.5 ± 3.5
4T1-rvLuc2	2D	69.3 ± 9.0	45 ± 3.0

The drug concentrations required to inhibit cell growth by 50% (IC_{50}) at 72h in HeLa cells, HeLa mEGFP-α-tubulin and mRFP-H2B cells (HeLa-EGFP/RFP), A549 cells, 4T1 mRFP-H2B cells (4T1-RFP) and 4T1-rvLuc2 cells cultured in 2D-monolayer (2D) or spheroids. Data represent the mean ± SD of three independent experiments, each performed in triplicate.

Table 2: PP-13 decreased the number of mice with thoracic and lymph node metastases

Treatments	Mice with thoracic metastases (day 14)		Mice with invaded lymph nodes (day 35)	
	Number	%	Number	%
Control	6/8	75	6/8	75
Paclitaxel 0.5 $mg.kg^{-1}$	3/8	37.5	5/7	71
PP-13 0.5 $mg.kg^{-1}$	5/8	62.5	4/8	50
PP-13 1 $mg.kg^{-1}$	4/8	50	1/8	13

Mice with 4T1-rvLuc2 tumors were treated with vehicle (control), paclitaxel 0.5 $mg.kg^{-1}$, or PP-13 (0.5 and 1 $mg.kg^{-1}$) (see Fig. 5D). Number and percentages of mice with thoracic metastases at day 14, and with invaded axillary and brachial lymph nodes at day 35 are shown in each group.

Table 3: Mice body-weight

Treatments	Mice body-weight at day 28 (%)	Mice body-weight at day 35 (%)
Control	118.75 ± 2.56	115.75 ± 3.57
Paclitaxel 0.5 $mg.kg^{-1}$	119.38 ± 1.41	111.29 ± 1.85
PP-13 0.5 $mg.kg^{-1}$	113.25 ± 0.86	108.25 ± 3.75 *
PP-13 1 $mg.kg^{-1}$	116.13 ± 1.84	116.13 ± 1.72

Mice with 4T1-rvLuc2 tumors were treated with vehicle (control), paclitaxel 0.5 $mg.kg^{-1}$, or PP-13 (0.5 and 1 $mg.kg^{-1}$) (see Fig. 5D). Mice body-weight is expressed as mean ± SEM (n=8, except in paclitaxel-treated group at day 35, n=7), and as percentage of initial body-weight (day 0). * p <0.05; two-way ANOVA with Bonferroni post-test (day 35 compared to day 28).

Table 4: Biochemical analyses of mice

Plasma biochemistry	Control (n=6) Mean ± SD	paclitaxel 0.5 mg.kg^{-1} (n=6) Mean ± SD	PP-13 1 mg.kg^{-1} (n=6) Mean ± SD
Potassium (mEq/L)	6.3 ± 0.8	6.6 ± 0.9	5.8 ± 0.8
Chloride (mEq/L)	113.2 ± 1.8	110.3 ± 3.4	113.0 ± 1.7
Calcium (mg/dL)	9.7 ± 0.3	9.6 ± 0.1	9.7 ± 0.4
Phosphorus (mg/dL)	8.2 ± 1.9	5.4 ± 0.2 *	6.5 ± 0.7
Glucose (g/l)	2.1 ± 0.4	1.6 ± 0.1 *	2.1 ± 0.3
Aspartate amino-transferase (UI/L)	201.5 ± 48.2	188.5 ± 56.4	205.7 ± 34.7
Alanine amino-transferase (UI/L)	33.3 ± 11.3	48.5 ± 10.4	38.0 ± 12.2
Alkaline phosphatase (UI/L)	52.5 ± 12.3	50.2 ± 9.3	58.5 ± 15.2
Total bilirubin (mg/dL)	0.2 ± 0.1	0.2 ± 0.2	0.2 ± 0.1
Total proteins (g/L)	42.0 ± 2.1	43.7 ± 1.9	43.7 ± 2.2
Albumin (g/L)	23.0 ± 1.5	23.8 ± 2.1	24.5 ± 2.3
Globulins (g/dL)	1.9 ± 0.2	2.0 ± 0.2	1.9 ± 0.1
Cholesterol (g/l)	0.7 ± 0.1	0.7 ± 0.1	0.8 ± 0.1
Triglycerides (g/l)	0.5 ± 0.1	0.6 ± 0.1	0.6 ± 0.1
Creatinine (mg/l)	9.7 ± 3.4	2.3 ± 0.5 *	4.0 ± 3.9
Blood Urea Nitrogen (g/l)	0.2 ± 0.02	0.2 ± 0.04	0.1 ± 0.02 *

Plasma biochemical values of mice after control, paclitaxel or PP-13 treatments were assessed. Data represent the mean ± SD of 6 mice per group. Data were analyzed using Mann-Whitney *U*-test. * Significant as compared to control group.

Table 5: Hematological and bone marrows analyses of mice

		Control (n=8)	paclitaxel 0.5 mg/kg (n=8)		PP-13 1 mg/kg (n=8)	
		Mean ± SD	Mean ± SD	*p* value	Mean ± SD	*p* value
Hematological analyses	Red blood cells (RBC) (T/L)	8.2 ± 0.6	7.2 ± 1.0	NS	7.6 ± 0.5	NS
	Haemoglobin (g/dL)	13.7 ± 1.0	12.4 ± 1.7	NS	13.2 ± 0.7	NS
	Haematocrit (%)	40.8 ± 3.3	35.5 ± 4.6	NS	38.1 ± 2.2	NS
	Mean corpuscular hemoglobin concentration (MCHC) (g/dL)	33.6 ± 0.5	35.0 ± 0.7	$p < 0.01$	34.5 ± 0.5	NS
	Mean Corpuscular Hemoglobin (MCH) (pg)	16.8 ± 0.4	17.2 ± 0.3	NS	17.3 ± 0.3	NS
	Mean corpuscular volume (MCV) (μM^3)	50.0 ± 1.2	49.2 ± 1.3	NS	50.3 ± 1.3	NS
	Red cell distribution *index* (RDI) (%)	15.0 ± 1.0	14.9 ± 0.8	NS	14. 6 ± 0.9	NS
	White blood cells (WBC) (G/L)	18.3 ± 3.5	11.8 ± 4.0	$p < 0.05$	17.0 ± 2.9	NS
	lymphocytes (% of WBC)	50.1 ± 8.2	39.1 ± 16.9	NS	47.5 ± 6.4	NS
	Monocytes (% of WBC)	23.9 ± 4.9	26.0 ± 6.6	NS	21.1 ± 1.2	NS
	Granular cells (% of WBC)	26.0 ± 4.0	35.0 ± 11.8	NS	31.1 ± 6.9	NS
Hematological analyses of the bone marrow	Cell abundance in the bone marrow[#]	2.4 ± 0.9	3.1 ± 0.4	NS	2.9 ± 0.7	NS
	Megakaryocytes	16.0 ± 6.5	28.7 ± 12.5	NS	18.0 ± 11.0	NS
	Granular line (%)	74.9 ± 9.0	63.4 ± 13.0	NS	65.3 ± 11.1	NS
	Erythroblastic line (%)	14.3 ± 9.6	22.1 ± 14.4	NS	28.6 ± 9.2	NS
	Lymphocytes (%)	6.1 ± 4.1	8.4 ± 3.4	NS	5.2 ± 3.6	NS
	Monocytes (%)	4.8 ± 2.7	6.1 ± 3.9	NS	2.8 ± 2.2	NS

Complete blood count and white blood cells count and evaluation of the global cell abundance and megakaryocyte and leukocyte counts in the bone marrow, from mice treated with control, paclitaxel, or PP-13. Data represent the mean ± SD of 8 mice per group. [#] from score 1 (low abundance) to score 4 (high abundance). Data were analyzed using one-way analysis of variance. NS: not significant.

Figure 1
Click here to download high resolution image

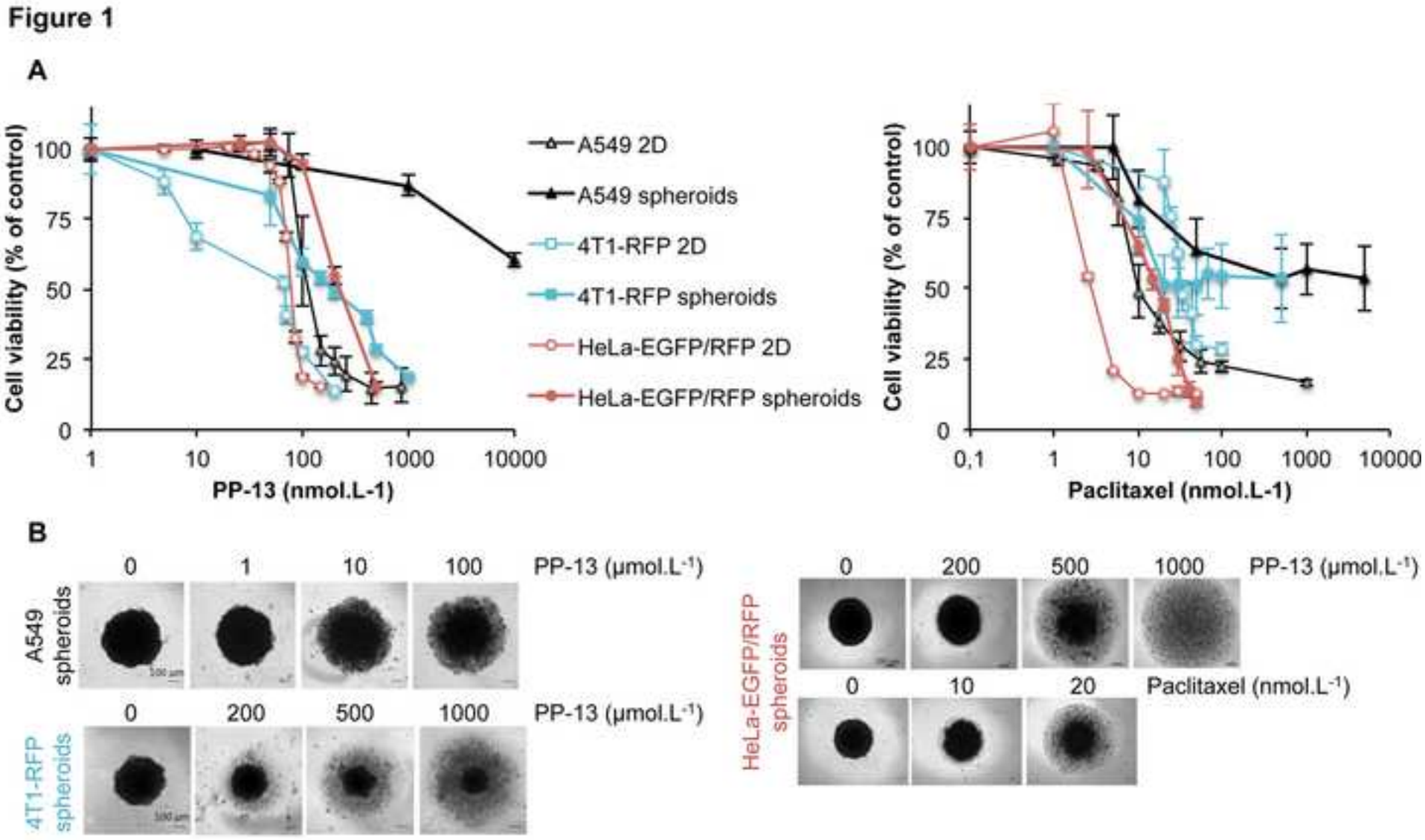

Figure 2

Click here to download high resolution image

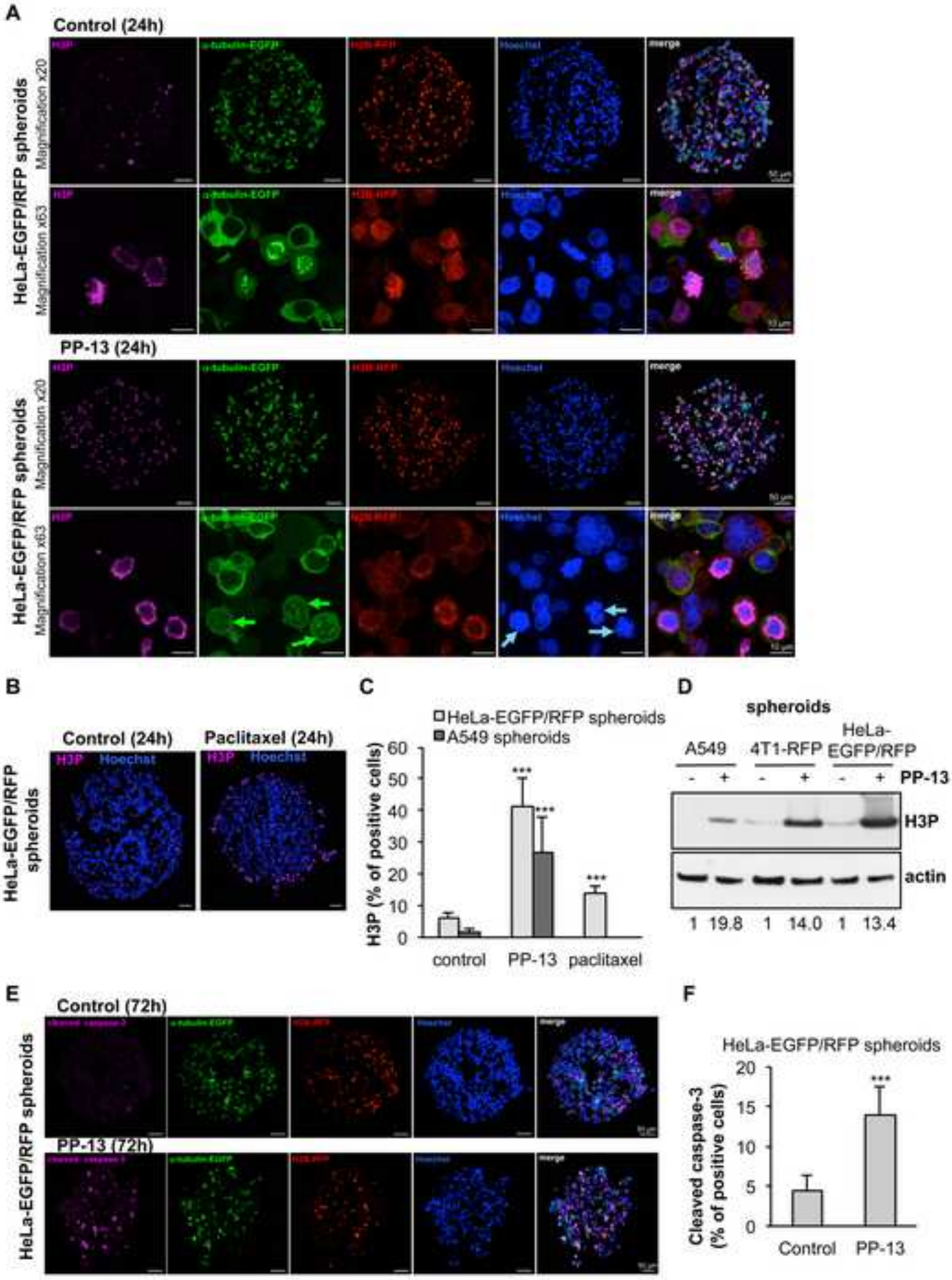

Figure 3

Click here to download high resolution image

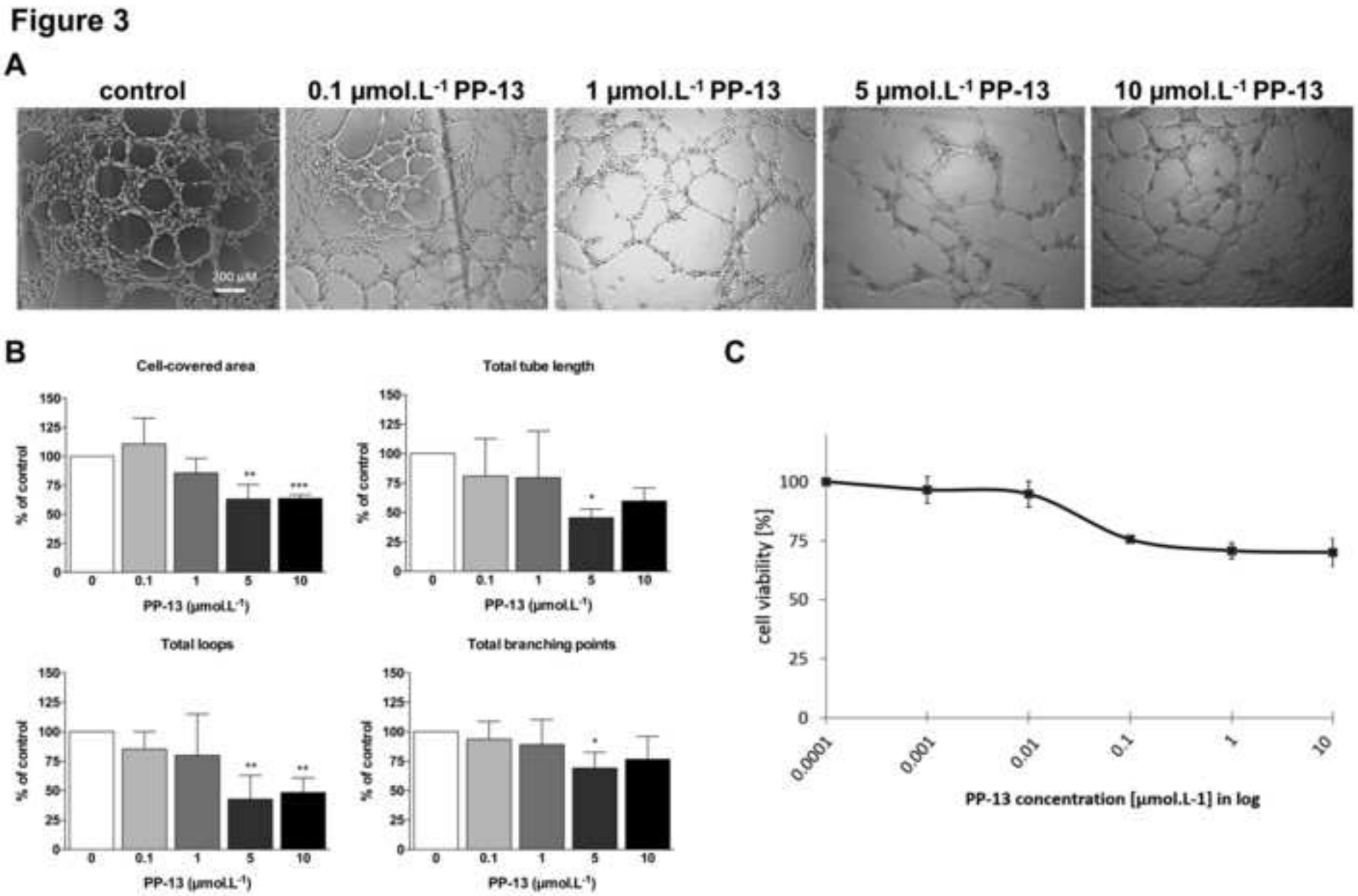

Figure 4

Click here to download high resolution image

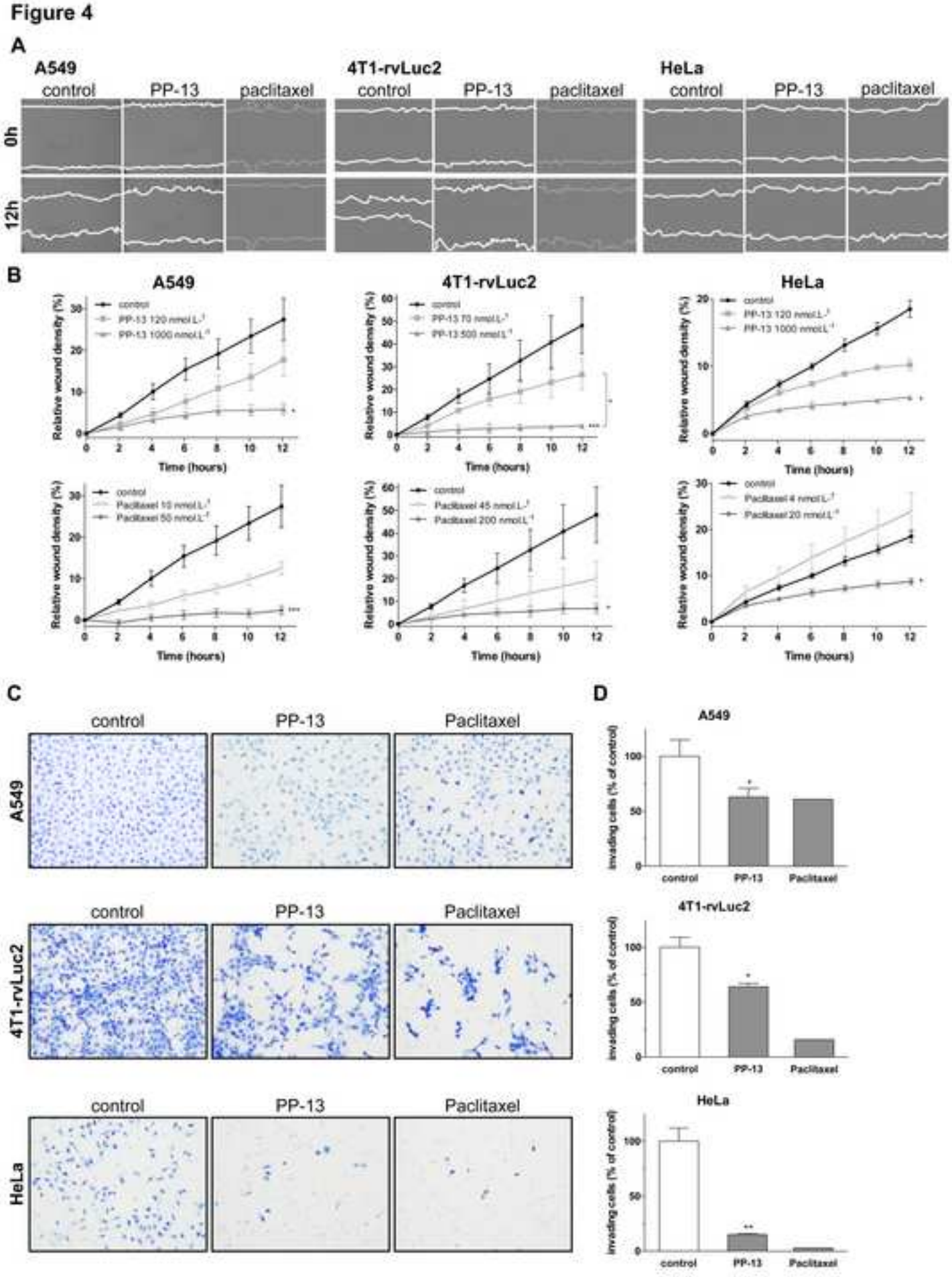

Figure 5

Click here to download high resolution image

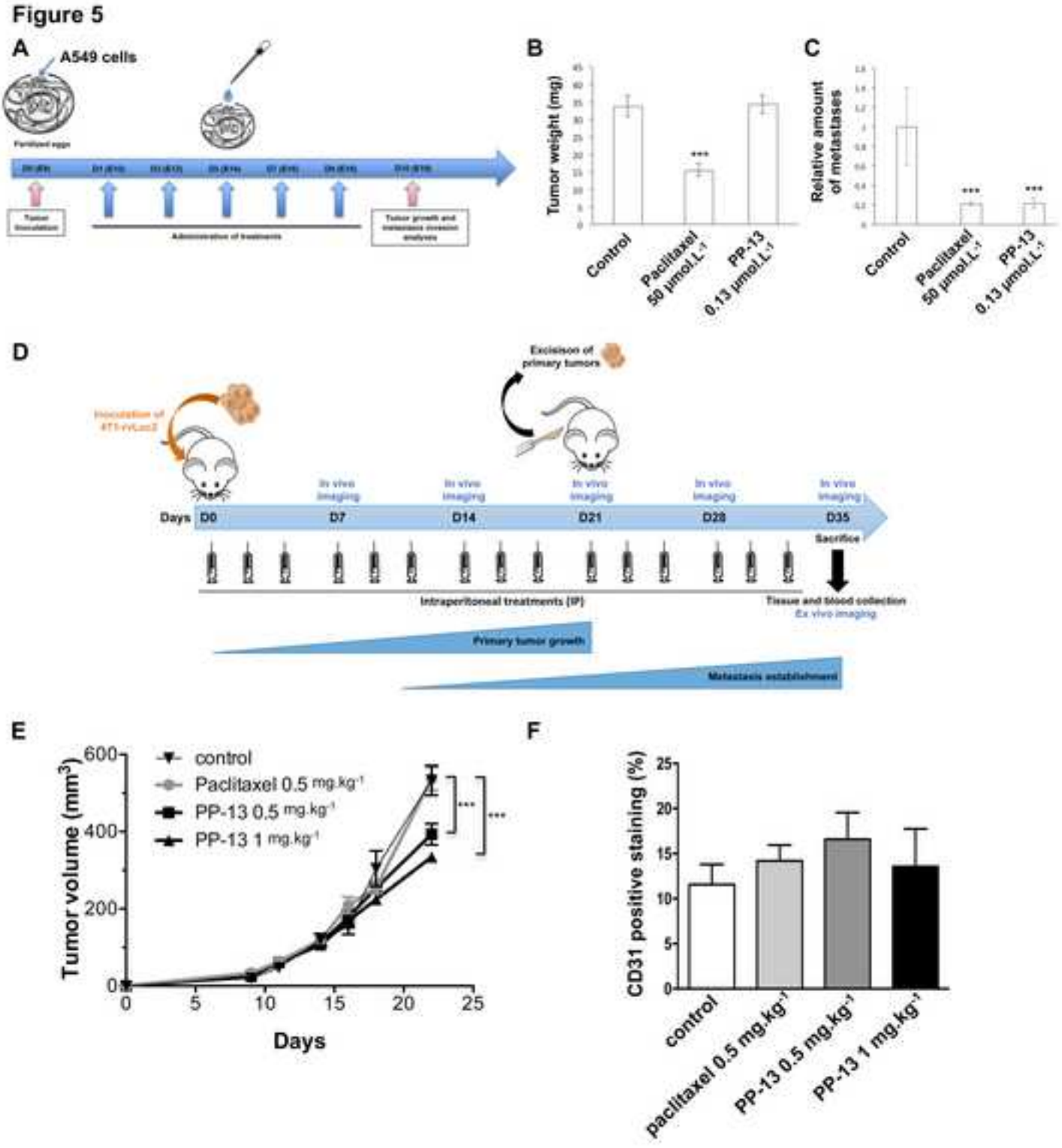

Figure 6

Click here to download high resolution image

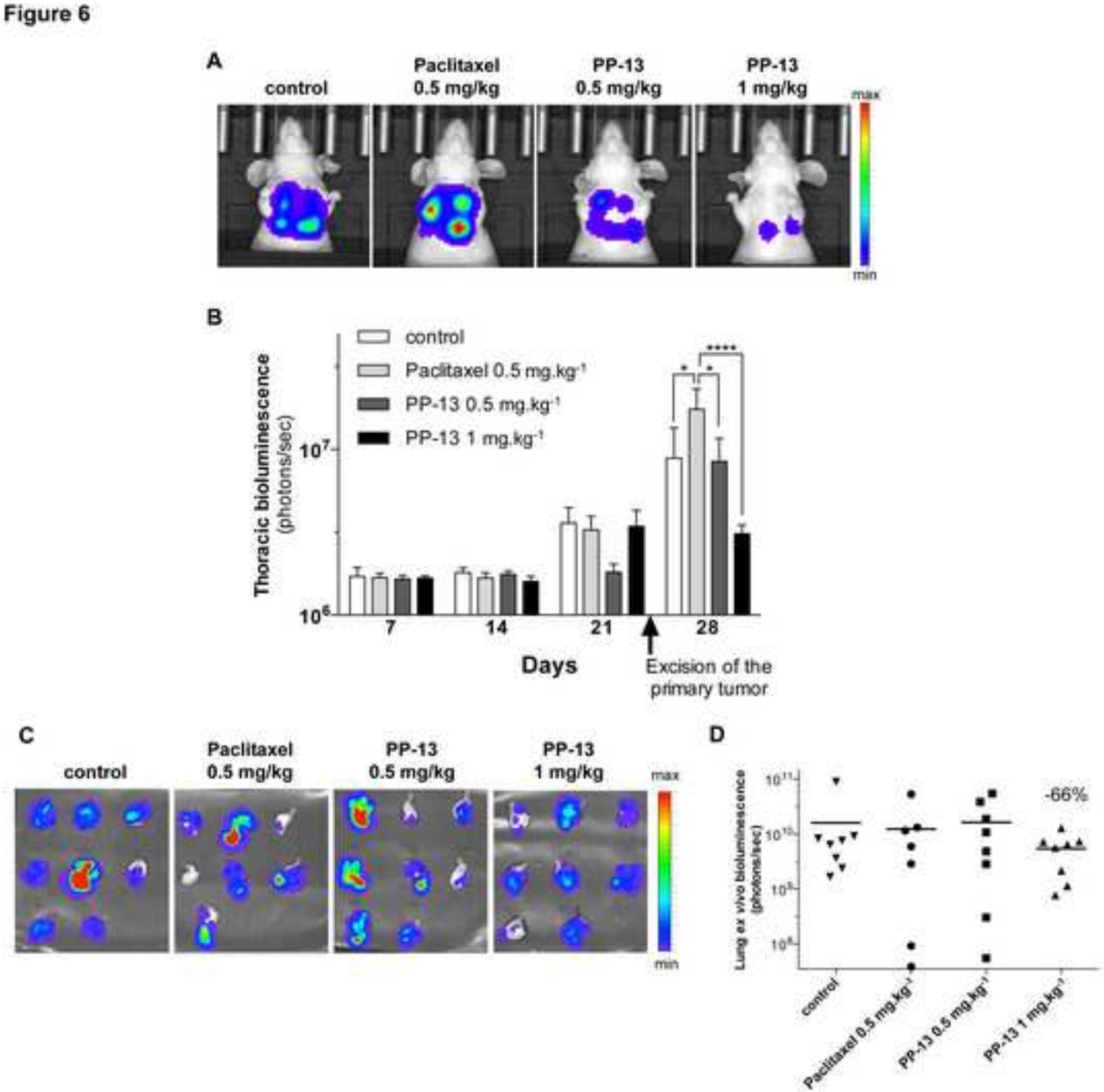

Figure 7

Click here to download high resolution image

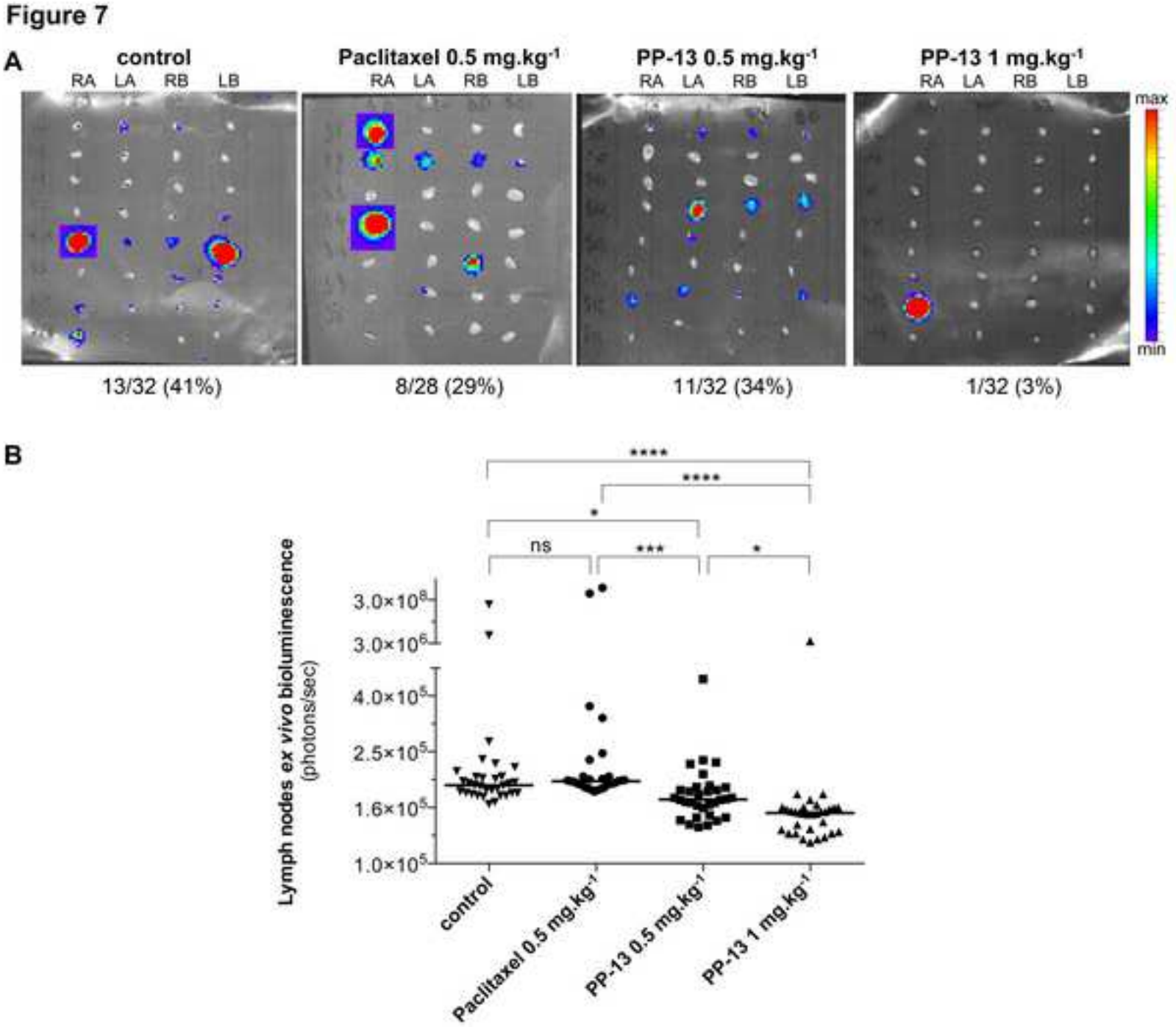

*Graphical Abstract (for review)

Click here to download high resolution image